Issue no. 2 · 2004
RSNA Edition

MAGNETOM FLASH

www.siemens.com/magnetom-world

Price 10,- EUR

Content

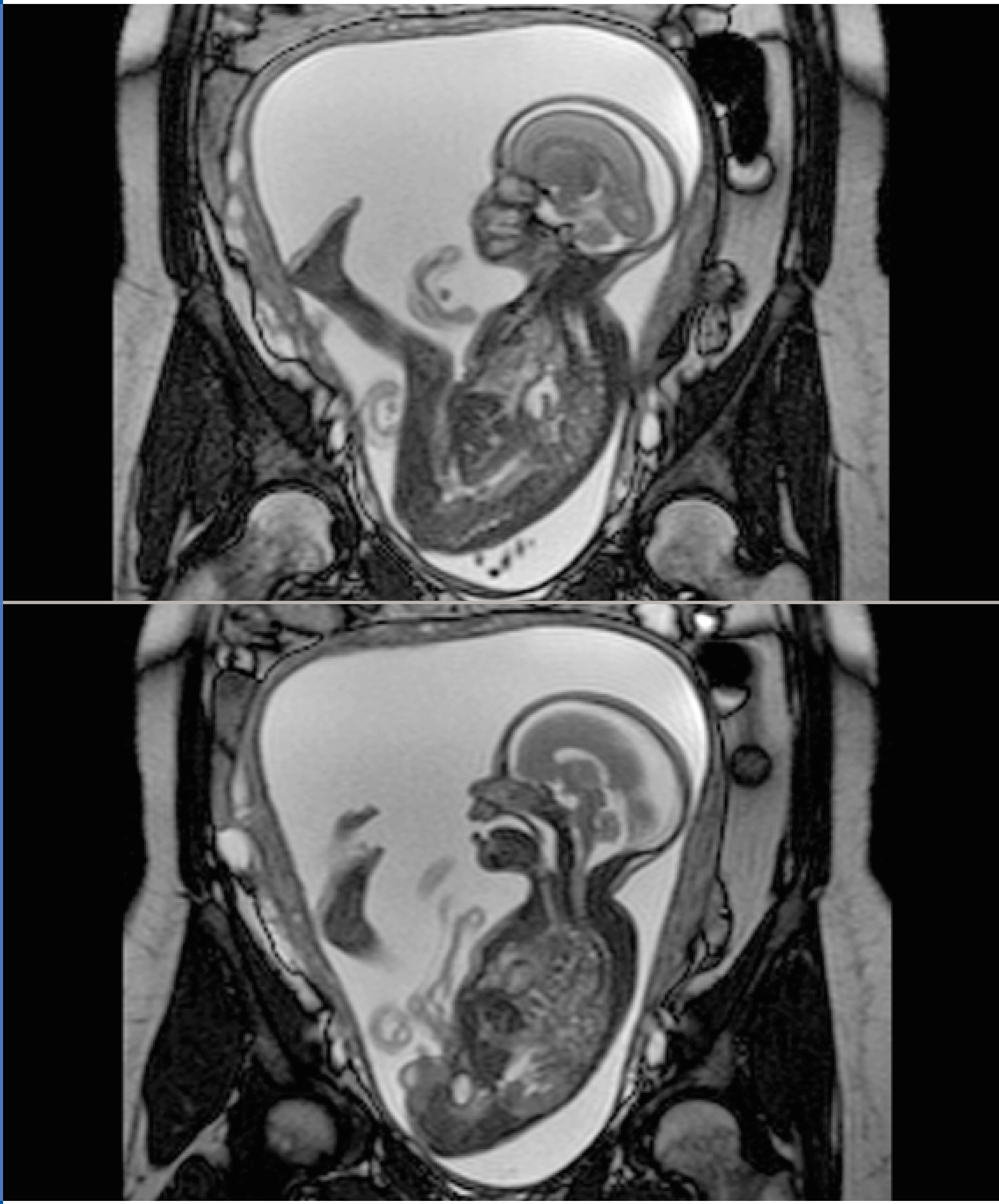

MAGNETOM Avanto
Case Reports

29

SIEMENS
medical

TECHNOLOGY

LIFE

The information presented in MAGNETOM Flash is for illustration only and is not intended to be relied upon by the reader for instruction as to the practice of medicine. Any health care practitioner reading this information is reminded that they must use their own learning, training and expertise in dealing with their individual patients. This material does not substitute for that duty and is not intended by Siemens Medical Solutions to be used for any purpose in that regard.

The drugs and doses mentioned in MAGNETOM Flash are consistent with the approval labeling for uses and/or indications of the drug. The treating physician bears the sole responsibility for the diagnosis and treatment of patients, including drugs and doses prescribed in connection with such use. The Operating Instructions must always be strictly followed when operating the MR System. The source for the technical data is the corresponding data sheets.

Farewell to all MAGNETOM Flash readers

For the last four years I have had the privilege and pleasure of working with the MR Division in Erlangen. Even though my specific assignments were related to the US MR group, on many occasions I have had the opportunity to work with others from around the world. One of these tasks was to assist the Editor of the MAGNETOM Flash with reviewing and editing articles for the periodical. I will no longer be able to participate in this function with my new assignment back within the US MR group in Malvern PA. I enjoyed working with the Flash very much since I know how important the magazine is to our readers around the world.

I have met many of our users during the last four years and several most recently at the MAGNETOM Summit meeting held in the beautiful Bavarian resort on the Tegernsee. There we listened to speakers and customers from around the world able and willing to share ideas and experiences with their MAGNETOM MR Systems. Experiences that ranged from early experiences with the MAGNETOM Avanto all the way to the futuristic views of Dr. Larry Wald and potential continuing developments through the RF technology.

The meeting was not all work: there was time to enjoy local food and fun in the Bavarian Alps high above the Tegernsee. It was truly a memorable event (did I really see people sniffing tobacco powder and then blow their nose in colored bandanas???) and I will always remember this World Summit as I hope will all of you.

Regarding my current status. I left the MR Marketing in Erlangen and returned to the US as of the first of September 2004, and since my return, I have hit the road running. I am very involved in the US product launch for the MAGNETOM Espree. The launch is actually a "roadshow" moving around the US from July to October.

The roadshow idea came about from the need to introduce our latest Tim product in the US without the advantage of a major trade show or other major event in which to show the product. The MAGNETOM Espree is situated in a mobile showroom that is taken from destination to destination including cities like New York, Cleveland, Omaha, Seattle, Las Vegas, Dallas and many others, where it is set up for customer events as well as local sales reps' training. The total of sixteen roadshows will end in Orlando to time with our National Sales Meeting.

Overall the roadshow has been very successful. We are confident that the Open Bore MAGNETOM Espree will have a perfect fit in the US Market and this is strengthened by the reactions of customer who have seen the system.

In closing I want to add my best regards to my Erlangen colleagues. I miss them very much. My past four years in Germany were an experience of a lifetime. It was as difficult to leave Germany as it was to leave my family and friends in the US when I first moved to Germany. But, I look forward to continuing my contact with as many of you as possible. There will be many opportunities for our paths to cross in the future.

Enjoy this issue of Flash.

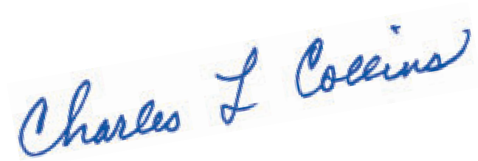

Charlie Collins, B.S.R.T.
Market Manager (USA),
Erlangen

Editorial Team

Editor's note:
We miss you a lot too Charlie...
I hope to see you and your family in Arkansas in the near future.
Good luck!

Charlie Collins in Malvern, PA, USA

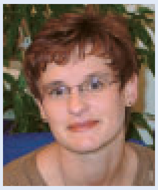

Marion Hellinger, MTRA
MR Marketing-Application Training, Erlangen

Lisa Reid,
US Installed Base Manager, Malvern, PA

Dagmar Thomsik-Schröpfer, Ph.D.
MR Marketing-Products, Erlangen

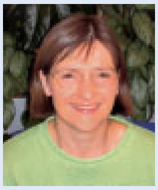

Antje Hellwich
Associate Editor

A. Nejat Bengi, M.D.
Editor in Chief

Achim Riedl
Technical Support, Erlangen

Milind Dhamankar, M.D.
Manager Clinical MR Research Collaborations, Siemens Medical Solutions USA

Tony Enright, Ph.D.
Asia Pacific Collaborations, Australia

Peter Kreisler, Ph.D.
Collaborations & Applications, Erlangen

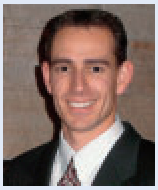

Stuart Schmeets
Advanced 3T Applications Specialist

Gary R. McNeal, MS (BME)
Advanced Application Specialist
Cardiovascular MR Imaging
Siemens Medical Solutions USA

We thank Mr. Lowrence Tallentire for this editorial help.

The World's First Open Bore, High-Field MRI Installed

Antje Hellwich

Siemens AG
Medical Solutions,
Magnetic Resonance Division,
Customer Care Manager,
Erlangen, Germany

Monday, September 20, 2004 MAGNETOM Espree – The world's first Open Bore, 1.5 Tesla MRI installed at Mayo Clinic, Jacksonville, Florida, USA.

Mayo Clinic is a multi-specialty medical clinic in Jacksonville, Florida. The staff includes 328 physicians who provide diagnosis, treatment and surgery working in more than 40 specialties. Patients who need hospitalization are admitted to nearby St. Luke's Hospital, a 289-bed Mayo facility.

70 cm + 125 cm + 1.5T + Tim

At Siemens Medical Solutions in Erlangen, Germany the challenge was not to make a more "open" Open, but to retain the performance of a 1.5T system in combination with the most open design possible. This combination of 1.5T, Open Bore, and Tim, the Total imaging matrix, is something only Siemens could do as Siemens is the only vendor designing and integrating magnets, gradients and RF-coils in-house.

At Mayo Clinic, Jacksonville, USA the challenge was not to decide for a patient friendly system with a very wide 70 cm bore, a very short 125 cm magnet and the powerful performance of 1.5T with Tim. The challenge was to find a day without hurricane warning to install the MAGNETOM Espree.

Combining what patients want with the features radiologists need.

MAGNETOM Espree offers, for the first time, **CT-like comfort** with its 70 cm patient bore and its short and open magnet. So it's head-out and feet first for most exams. Perfect for obese and claustrophobic patients.

To make the examination quick and comfortable for the patient, MAGNETOM Espree – a Tim system – combines up to 76 seamlessly integrated matrix coil elements and up to 18 RF channels to create one Total imaging matrix. This means only one set-up of coils, no patient repositioning and no coil repositioning.

When scanning large anatomical areas with the seamlessly integrated Matrix coils you will get highest signal to noise and local coil image quality without restriction in coverage.

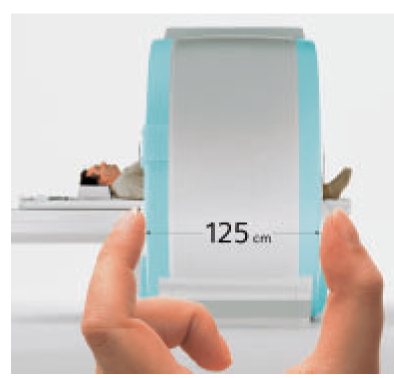

"This is going to increase our efficiency and patient convenience," says Dr. Jerald Pietan, chair of Mayo's Department of Radiology. "The patient-friendly design of this magnet will make it easier for large patients and those with claustrophobia to have an MRI examination which produces quality images. This can reduce the need to repeat and interrupt exams."

At Mayo Clinic creativity in using the new dimensions in MR has gone sky high. Their MAGNETOM Espree is used for routine orthopedic imaging e.g. wrist imaging: here the face down Superman position so far used for wrist imaging might be superseded by the patient sitting comfortably at the end of the magnet with his/her arm extended horizontally into the magnet.

Or for long bones and entire extremity scanning: Without MAGNETOM Espree the technologists would scan thighs then calves or upper then lower arms and these would be read as separate series. With their new seamless anatomical coverage these separate scans are a thing of the past. The same is true for spine imaging.

But leaving aside their creativity, the mere patient friendliness of its new system could gain Mayo Clinic up to 400 additional referrals a year from orthopedic surgeons if claustrophobic concerns are alleviated. Not to mention obese patients. Obesity is increasing worldwide. Every fifth adult is considered obese in the UK and the rate is even higher in the US. This results for the United States alone in 44 million patients who have only limited access to high-field MR so far, but a high risk for cardiovascular diseases and orthopedic distortions. Currently, patients too large to fit inside the bore of a high-field MRI magnet have image studies done in open MRI-systems with low-field magnets. Now MAGNETOM Espree features almost one foot (30 cm) of free space between a patient's head and the magnet. With the shortest 1.5 Tesla magnet now available more than 60% of exams can be completed with the patient's head outside the bore, helping to ease claustrophobia.

On the technical side MAGNETOM Espree is available with Tim [32 x 8]

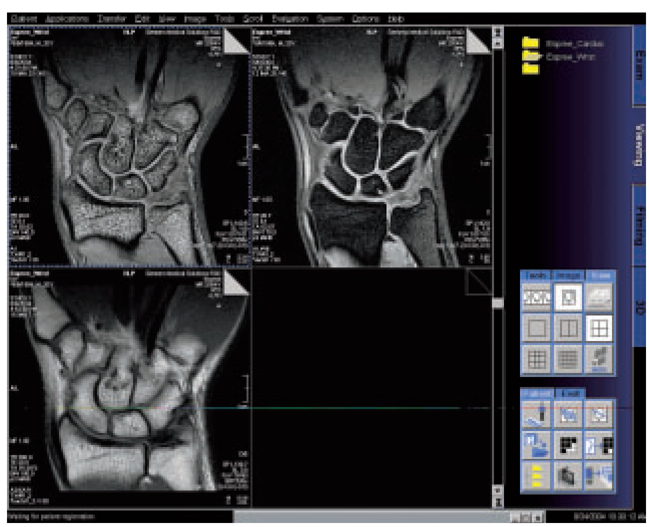

Wrist images.

Whole spine image.

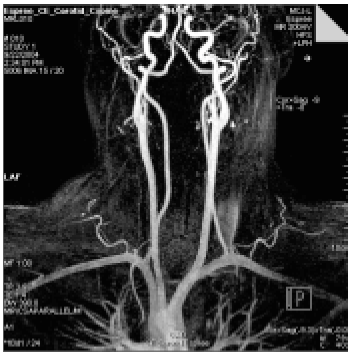

Carotid MRA with coverage from aortic arch to circle of Willis.

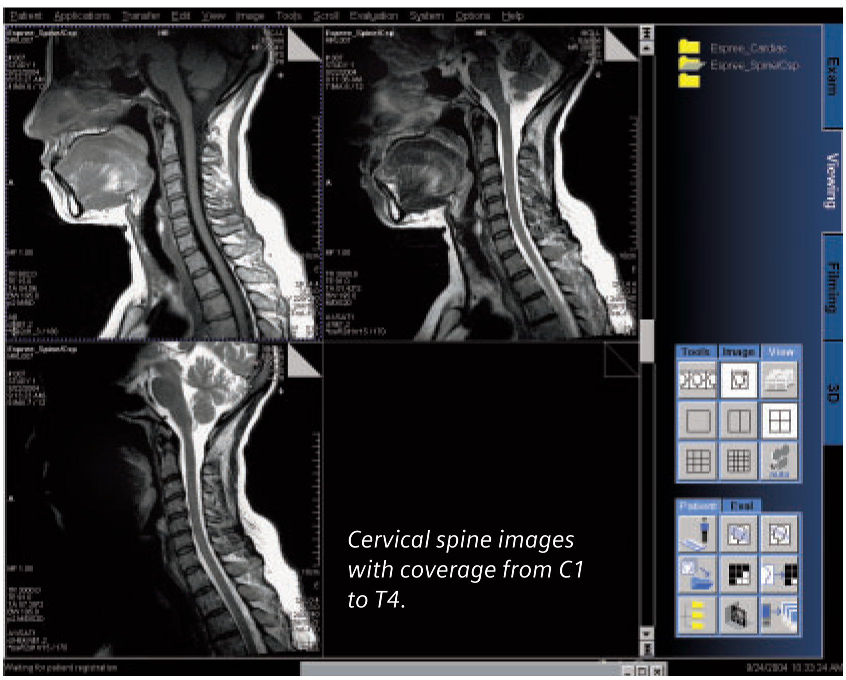

Cervical spine images with coverage from C1 to T4.

or with Tim [76 x 18]. And it comes with a Z-engine (33 mT/m, SR 100 T/m/s) gradient system.

Tim is the ideal solution for MAGNETOM Espree. Its Matrix coils can be combined seamlessly to achieve large coverage and high-resolution images without sacrificing signal-to-noise. Tim ensures higher SNR, enabling best image quality even with highest PAT factor. For studies ranging from clinical routine up to advanced applications such as tumor staging.

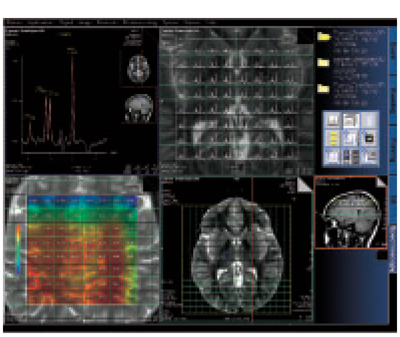

CSI spectroscopy.

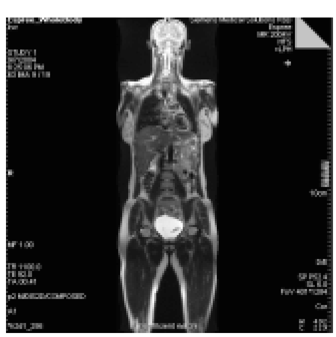

Whole body imaging with MAGNETOM Espree.

MAGNETOM Espree – Revolutionary workflow

Surrounding MAGNETOM Espree are a whole group of innovations that will not only change the way you work. But are surprisingly easy to work with. Of course, you have already met Tim and know that it will help to accelerate patient setup, scan times and exams. But there is more.

- **Inline Technology enables real-time processing.** Eliminating many manual steps. Get immediate clinical results for prospective motion correction (PACE), diffusion, perfusion, and MRI angiograms.
- **Phoenix, unique to Siemens,** gives you superior reproducibility based on a one-click drag & drop of images, not on protocols.
- Another innovation for MRI workflow is **AutoAlign™** which **enables automatic slice positioning.** Delivering highest reproducibility with uniform consistent results, even with new staff.
- And, helping to make it easier than ever to get patients ready for exams is **Intelligent Coil Control.** With Automatic Coil Position Detection of all coil elements both fixed and flexible, you're just a click away from faster exam set-up with little interaction.

The second MAGNETOM Espree is up and running at the Turville Bay MRI Centers in Madison, Wisconsin, USA.

MAGNETOM Espree

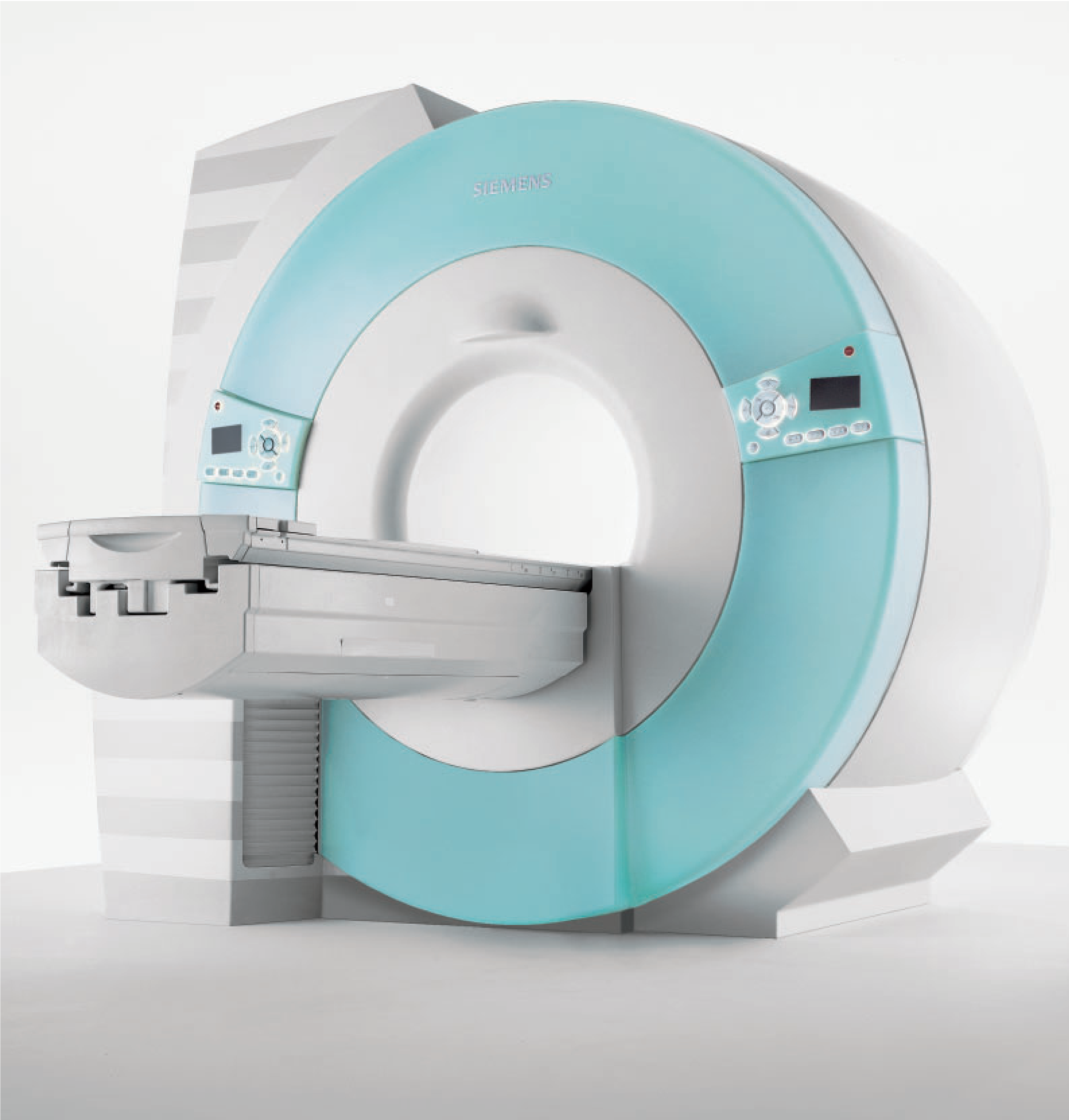

MAGNETOM C! ...
...is Changing the Face of Mid-Field MRI

Stefan Domalski

Siemens AG
Medical Solutions,
Magnetic Resonance Division,
Market Segment Manager Open Systems, Erlangen, Germany

MAGNETOM World Events around the globe

On July 19, 2004 a new member of the MAGNETOM family achieved US market clearance – MAGNETOM C! – the first open MAGNETOM operating at 0.35T. It is also a member of the MAGNETOM Open family together with the 0.2T MAGNETOM Concerto and the 1.5T MAGNETOM Espree.

The first MAGNETOM C! installed in Europe being delivered to the Eduardus Hospital in Cologne, Germany.

The MAGNETOM C! is an open MRI system based on over 25 years of Siemens MR experience, following the tradition of spearheading the innovations in open MRI. A high-field gradient system with 24 mT/m and a true multi-channel RF system with up to four channels and coils able to cover up to 100 cm (25”) field of view are built into the most compact magnet in mid-field, reducing claustrophobia to the minimum. The system is equipped with iPAT parallel acquisition techniques and multi-directional motion correction 2D PACE for fast and robust examinations.

The MAGNETOM C! was introduced to the MR community during a global series of MAGNETOM World events that began in July at the Caravelle Hotel in Ho-Chi-Minh City, Vietnam, where 86 MR experts from all over Asia were the first to see the new system and its potential.

The first MAGNETOM C! in Asia was installed at the Airforce General Hospital in Beijing, China in June 2004. Following the first clinical studies, 150 guests were invited to its official inauguration at the Shangri-La hotel in Beijing, at which Prof. Zhang Wanshi shared his initial experiences of working with the new system. MR users from all over the world have taken the opportunity to check out the MAGNETOM C! in Beijing in the first couple of months after installation and appreciated the exceptional image quality and easy handling of the system.
The HOSPEQ exhibition at the Beijing exhibition center was the first trade show world-wide featuring the MAGNETOM C!

In Europe, the first MAGNETOM C! was installed on September 4 at the Eduardus Hospital in Cologne, Germany, while the first US system went to the Physicians Imaging Center in Dallas, Texas.

This before meeting the public at the “Open MRI in Clinical Practice” meeting in Las Vegas, Nevada, side by side with the MAGNETOM Espree.

The MAGNETOM C! has been developed and is manufactured at the new Siemens MR facility in Shenzhen, China – evidence of the Siemens philosophy of being close to customers anywhere in the world. In addition to research, development and manufacturing, a Headquarter Support Center (HSC) for MR will be set up in Shenzhen, complementing the two existing centers in Erlangen, Germany and Cary, North Carolina, USA with a center in the Asian time zone. The center in Shenzhen has started operations and supports not only the MAGNETOM C! but also all other MAGNETOM systems.

The MAGNETOM C! was introduced to the customers in USA with a presentation at the Open MRI in Clinical Practice Meeting and a reception at the Hard Rock Hotel.

MAGNETOM C! appearing from a cloud of mist and lights at the inauguration event at the Shangri-La Hotel, Beijing, China on Aug 7, 2004.

Delegates at the MAGNETOM C! inauguration meeting on June 12, 2004 at the Caravelle Hotel in Ho-Chi-Minh City, Vietnam.

Prof. Zhang Wanshi from Airforce General Hospital in Beijing, China in front of his new MAGNETOM C!, the first system in the world was installed in June 2004.

T2 TSE Restore, 3 steps, 512 matrix, 345 mm FoV, SL 4.0 mm.

T2 TSE Restore, 512 matrix, 280 mm FoV, SL 3.0 mm.

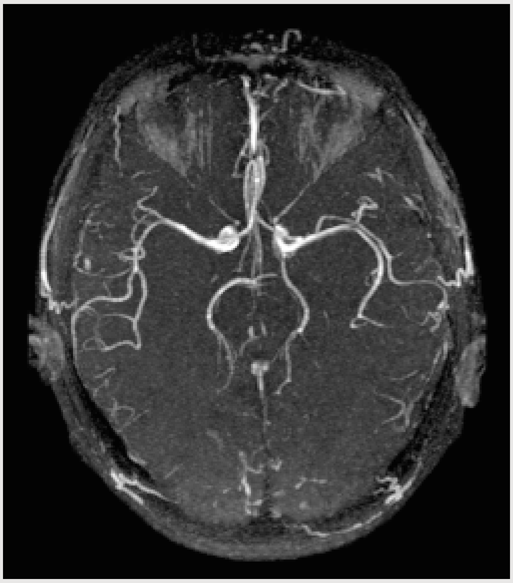

3D MIP, FLASH 2D, 512 matrix, 221 mm FoV, SL 78 mm.

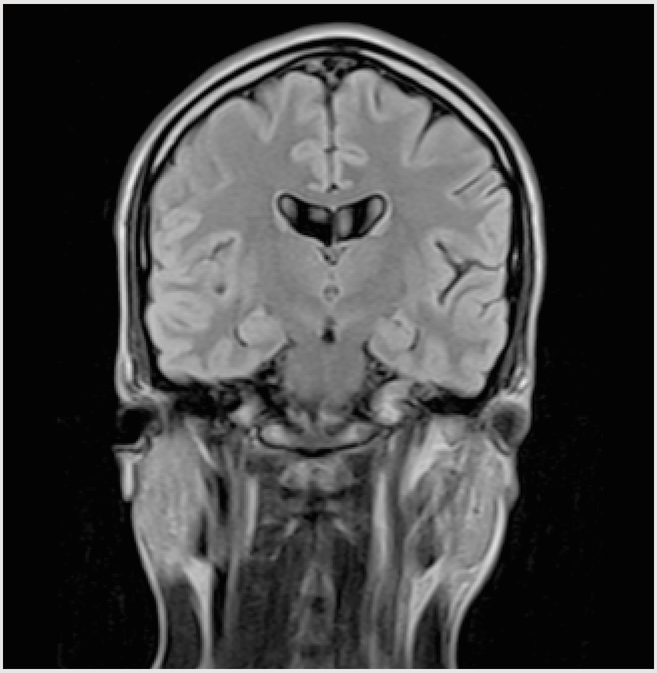

TIRM Dark Fluid, 512 matrix, 239 mm FoV, SL 5.0 mm.

MAGNETOM C!

Image Gallery

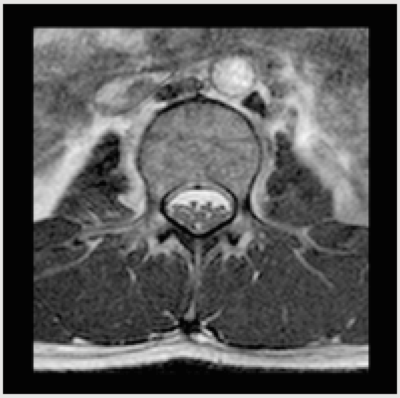

3D CISS, 512 matrix, 216 mm FoV, SL 3.0 mm.

TrueFISP 2D, 256 matrix, 263 mm FoV, SL 8.0 mm.

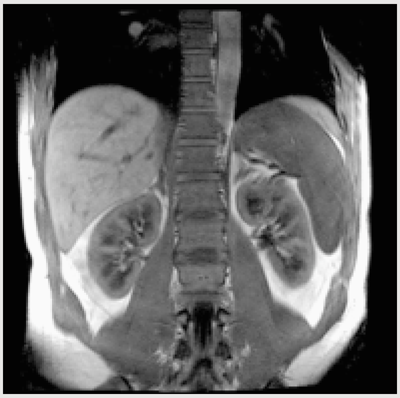

FLASH 2D, 512 matrix, 363 mm FoV, SL 6.0 mm.

FLASH 3D we, 384 matrix, 146 mm FoV, SL 3.5 mm.

TSE Restore, 640 matrix, 250 mm FoV, SL 4.0 mm.

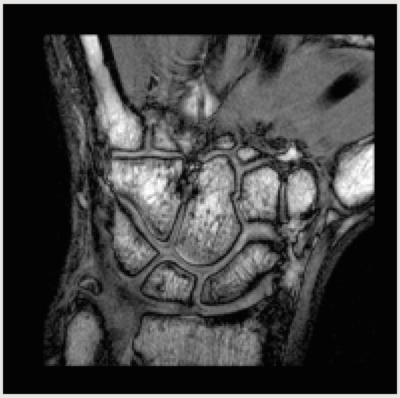

3D DESS, 512 matrix, 115 mm FoV, SL 2.0 mm.

TSE Restore, PAT x 2, 512 matrix, 180 mm FoV, SL 4.0 mm.

FLASH 2D we, 256 matrix, 160 mm FoV, Courtesy of Eduardus Hospital, Cologne, Germany.

TSE Restore, 512 matrix, 300 mm FoV, SL 4.0 mm, Courtesy of Prof. Zhang Wanshi, Airforce General Hospital, Beijing, P.R. China.

FLASH 2D we, 256 matrix, 160 mm FoV, SL 4.0 mm, Courtesy of Eduardus Hospital, Cologne, Germany.

3D MRCP with 2D PACE multi directional motion correction algorithm, Courtesy of Hai Nan Nong Ken Sanya Hospital, P.R. China.

Cine FLASH 2D with tagging, Courtesy of Prof. Zhang Wanshi, Airforce General Hospital, Beijing, P.R. China.

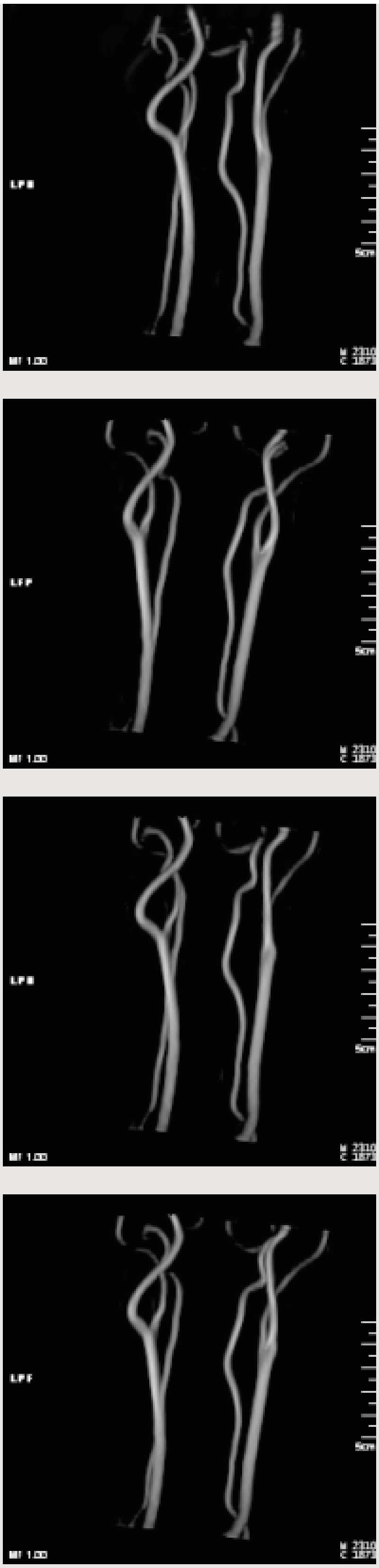

3D MIP, FLASH 2D, Hui Yang No. 1 People's Hospital, Hui Yang, P.R. China.

MAGNETOM C!

Image Gallery

FLASH 2D, 512 matrix, 350 mm FoV, SL 8.0 mm, Courtesy of Hui Yang No. 1 People's Hospital, Hui Yang, P.R. China.

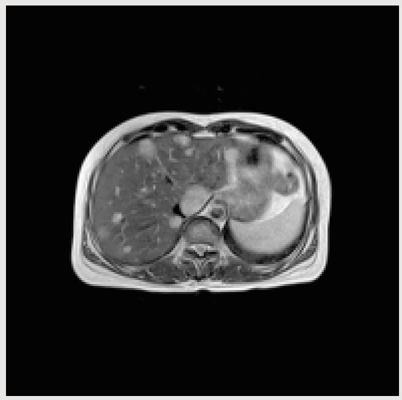

Triple contrast TSE, 512 matrix, 350 mm FoV, SL 10.0 mm, Courtesy of Hui Yang No. 1 People's Hospital, Hui Yang, P.R. China.

3D HASTE, 192 matrix, 250 mm FoV, SL 8.0 mm, Courtesy of Hui Yang No. 1 People's Hospital, Hui Yang, P.R. China.

TSE Restore with PAT x 2, 256 matrix, 260 mm FoV, SL 4.0 mm in 2:11 min.

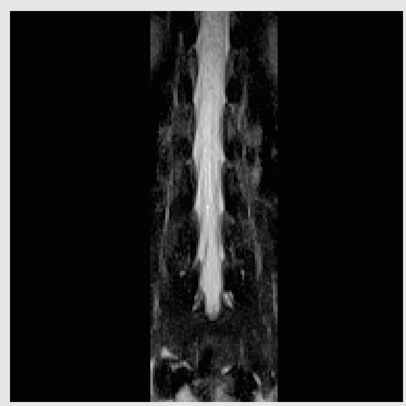

3D MIP of 3D HASTE, 192 matrix, 250 mm FoV, SL 45 mm.

Case Report: MRCP and MR of the Liver (Pre- and Post-Contrast Examinations)

Michael Fenchel, M.D.
Ulrich Kramer, M.D.
Katrin Tomaschko
Heinz-Peter Schlemmer, M.D.

University Hospital Tübingen,
Dept. of Radiology
Tübingen, Germany

Patient History

47 year old male patient with known Klatskin tumor (stage III).

MR images were performed to assess the vascular status of the abdomen and to rule out a pyelothrombosis.

Examination

Examination was performed on a 1.5T Siemens **MAGNETOM Avanto** scanner using a Body Matrix coil.

20 minutes before starting the examination, 300 ml of Lumirem (iron-oxide) were administered p.o. to reduce intraluminal signal from duodenum. Immediately before the MRCP (MR Cholangiopancreatographie) examination, 40 mg of butylscopolamide (Buscopan, Boehringer, Germany) were administered intravenously to suppress bowel peristalsis.

Images depicting the abdominal anatomy were acquired using a coronal HASTE, an axial navigator triggered fat suppressed T2-weighted TSE sequence and a T1-weighted breath-hold FLASH 2D sequence.

MRCP was performed using a coronal, heavily T2-weighted TSE 3D sequence with PACE enabling free breathing of the patient during the examination. MR images were post-processed subsequently using a maximum intensity projection (MIP) algorithm.

2 ml Gadolinium-DTPA were injected as test bolus to measure the circulation time. A coronal angulated FLASH 3D sequence in breath-hold technique was used to acquire pre and post contrast images. The scan delay was calculated according to the following formula: circulation time – time to center of k-space + 4 [s].

Contrast agent dose was 0.15 mmol Gd-DTPA/ kg body weight. Two sets of post contrast data were acquired. Furthermore, axial fat suppressed FLASH 2D post contrast images were recorded.

Findings

1. Klatskin tumor (size 4.2 x 3.0 cm) with potential infiltration of the portal venous system in the right lobe of the liver.
2. Occlusion of the right portal venous branch in the region of the tumor.
3. Infiltration of right and left hepatic arteries without affecting the bile ducts in this area.
4. Intrahepatic cholestasis particularly in the right lobe of the liver.

FLASH 3D

FLASH 3D

FLASH 3D

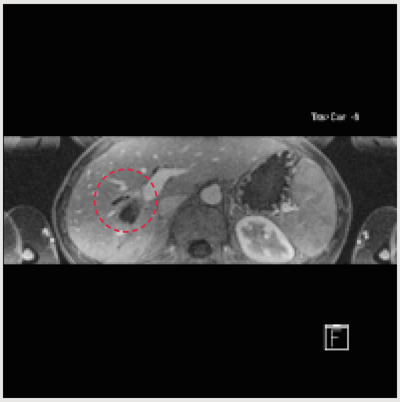

FLASH 3D

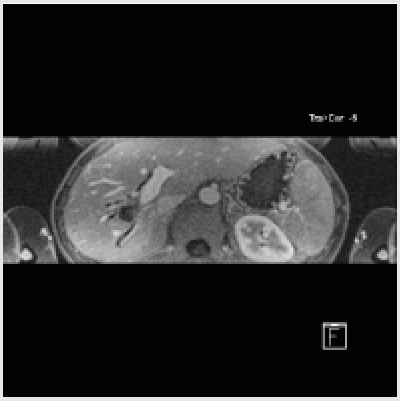

FLASH 3D

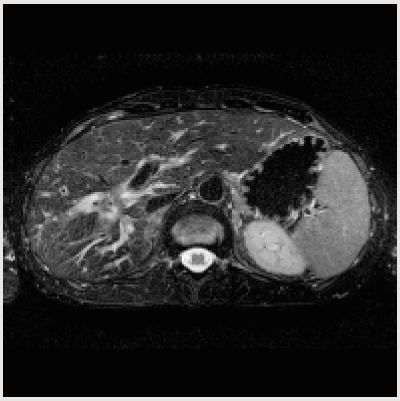

T2_TSE_fs

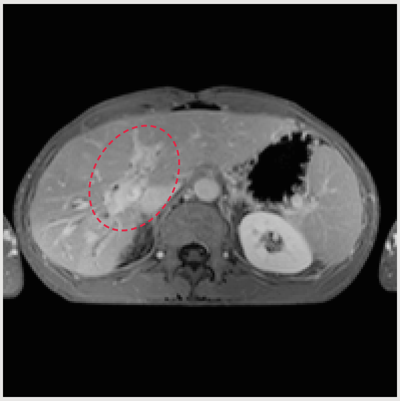

FLASH 2D_fs

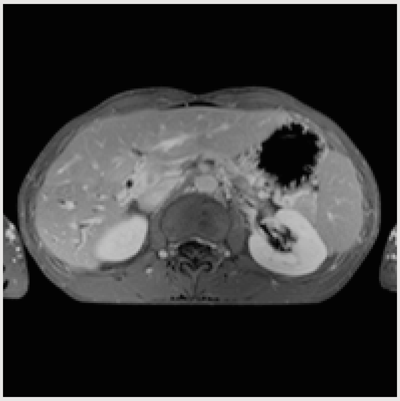

FLASH 2D_fs

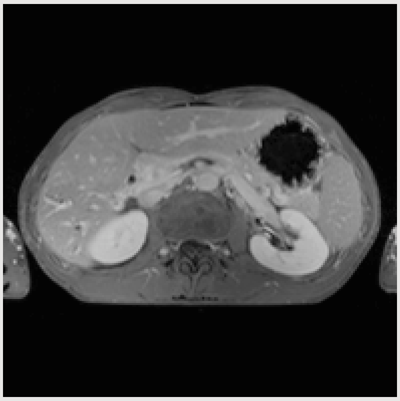

FLASH 2D_fs

MRA arterial phase.

MRA portal venous phase.

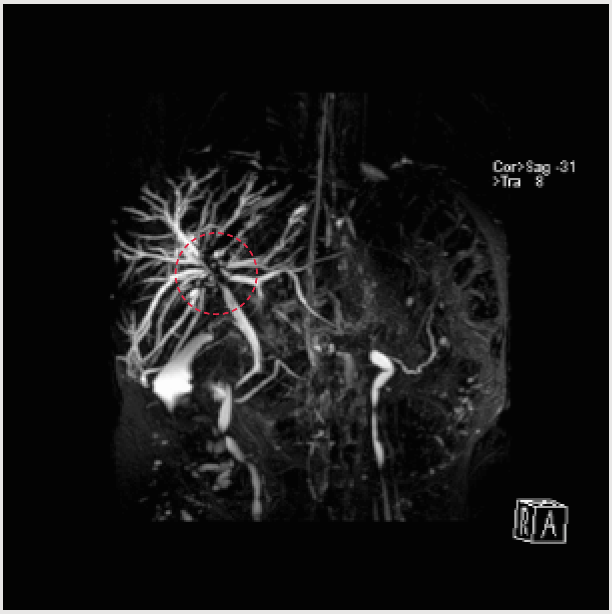

MRCP MIP image, TSE 3D.

MRCP MIP image, TSE 3D.

Case Report: Prenatal Diagnosis of Diaphragmatic Hernia

Ulrich Kramer, M.D.
Michael Fenchel, M.D.
Katrin Tomaschko
Heinz-Peter Schlemmer, M.D.

University Hospital Tübingen, Dept. of Radiology
Tübingen, Germany

Patient History

Fetus in the 26th week of gestation (36 year old mother) with history of known situs inversus and sonographic suspicion of atrial septum defect and diaphragmal hernia. MR imaging was requested to confirm the suspicion of diaphragmal hernia for planning surgery.

The safety of imaging (fetuses, infants) has not been established.

Examination

Examination was performed on a 1.5T Siemens **MAGNETOM Avanto** scanner using two Body Matrix coils. Mother's position was oblique to the left side to reduce compression of the inferior vena cava by the fetus leading to reduced venous flow to the right atrium. In order to reduce artifacts due to movement of the fetus, sedation was accomplished by oral administration of 5 mg diazepam prior to the examination.

First, localizer images were acquired to find the correct angulation for coronal and sagittal slices in the fetus. Subsequently, TrueFISP sequences were used to get anatomical coverage of thoracic and abdominal structures of the fetus. Representative angulations were repeated with T2-weighted TSE sequences to demonstrate the findings with increased resolution.

Sequences

HASTE (sagittal):
FoV: 217 x 290 mm,
slice thickness: 4 mm,
matrix: 328 x 512 mm,
flip angle: 150°, TR: 1310 ms,
TE: 74 ms, BW: 630 Hz/Px

TrueFISP (coronal and sagittal):
FoV: 325 x 400 mm,
slice thickness: 4 mm,
matrix: 156 x 256 mm,
flip angle: 69°, TR: 4.3 ms,
TE: 2.0 ms, BW: 490 Hz/Px.

T2w TSE (sagittal):
FoV: 218 x 290 mm,
slice thickness: 4 mm,
matrix: 180 x 320 mm,
flip angle: 150°, TR: 3940 ms,
TE: 103 ms, BW: 260 Hz/Px,
ETL = 23, Av = 3

Findings

The fetus presented with pelvic orientation, the placenta was situated ventrally. Situs inversus presenting with a left sided liver was detected. Mesenterial structures were detected in the dorsal mediastinum predominantly on the left side. The volume of the left lung was considerably reduced secondary to compression by intestinal structures. Urogenital structures and urinary bladder appeared normal.

Discussion

High resolution fetal MRI could easily be performed in a case with situs inversus demonstrating a large diaphragmal defect with left sided dystopia of abdominal structures in the mediastinum and consecutive lung compression. This crucial information was needed for further therapy planning because surgery is indispensable in this case to keep the baby alive after delivery.

TrueFISP

TrueFISP

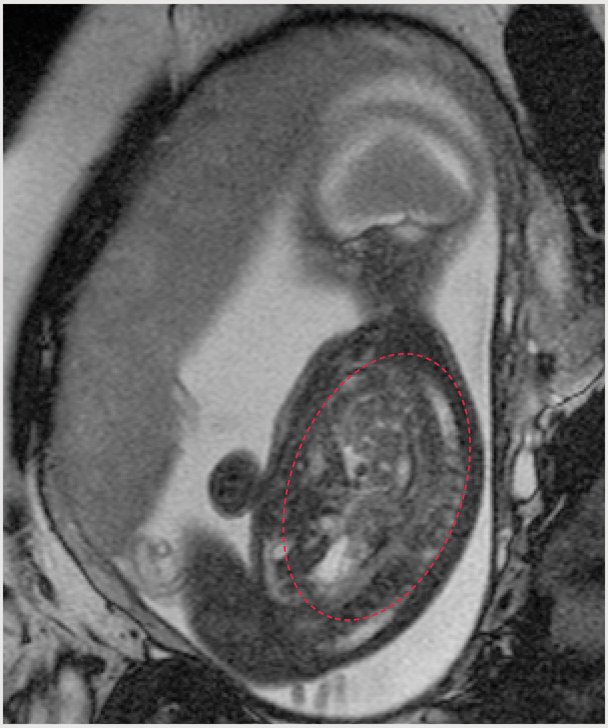

TrueFISP

The safety of imaging (fetuses, infants) has not been established.

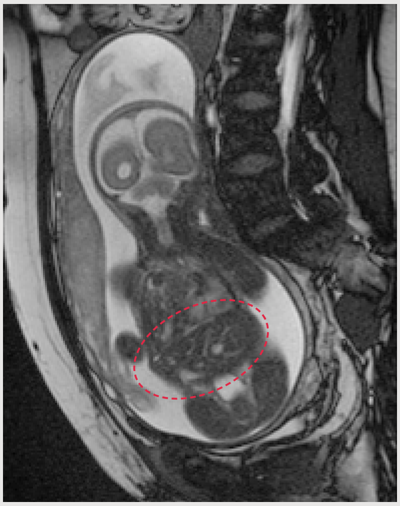

TrueFISP

TrueFISP

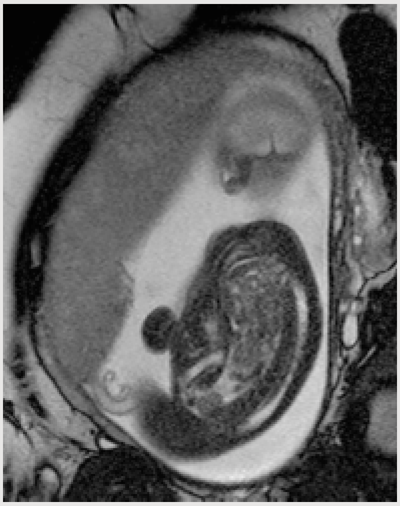

TrueFISP

TrueFISP

HASTE

The safety of imaging (fetuses, infants) has not been established.

Case Report: MRI of the Thorax

Michael Fenchel, M.D.
Ulrich Kramer, M.D.
Katrin Tomaschko
Heinz-Peter Schlemmer, M.D.

University Hospital Tübingen,
Dept. of Radiology,
Tübingen, Germany

Introduction

Carney's triad was described in 1997 in two young female patients presenting with gastric leiomyosarcoma, paraganglioma outside the adrenal gland, and pulmonary chondroma [1]. Typically, manifestation of this disease occurs in early adulthood whereas specific tumor entities may develop over years or decades. Gastrointestinal tumors which are part of the syndrome are especially hazardous for the patient and require early resection.

Patient History

26 year old female patient with known Carney's triad status post gastrointestinal tumor excision.

Conventional contrast-enhanced CT was done to assess pulmonary nodules which were detected first on conventional plain films; MRI was also acquired to rule out a suspicious tumor in the oesophagus and to compare the findings with the CT.

Examination

Examination was performed on a 1.5T Siemens **MAGNETOM Avanto** scanner using a Body Matrix coil.

Images were acquired during breath-hold after deep inspiration without ECG triggering.

First, transversal imaging was performed using a T2-weighted STIR, a T1-weighted FLASH 2D and a PD weighted volumetric interpolated 3-dimensional breath-hold (VIBE) sequence with fat saturation. Axial images based on the VIBE sequence were also used for coronal reconstruction.

2 ml Gadolinium-DTPA were injected with high flow to measure the circulation time. Subsequently, a coronal FLASH 3D with 128 slices per slab, slice thickness = 1.0 mm and an acquisition time of less than 20 seconds was measured before and after bolus injection of 0.15 mmol Gd-DTPA/kg body weight. Angiographic images were acquired during end-expiratory breath holding in order to improve image quality of subtracted images.

After contrast administration axial Flash 2D and VIBE sequences were repeated with fat saturation.

Findings

Multiple pulmonary lung nodes were clearly demonstrated in the right lung corresponding to the known chondromas. A tumor of the esophagus was not detected. The contrast enhanced MR angiography showed no abnormality.

Discussion

Carney's triad [1] is a rare disease with approximately 60 cases worldwide. A genetic disorder was suspected, although up to now this could not be confirmed. The detection of the tumors is essential for prognosis and therapy of patients, which necessitates early diagnosis. Gastrointestinal tumors are part of the syndrome and hazardous for the patient. MRI can be helpful in visualizing intrapulmonary chondromas, which supports the diagnosis, and for visualizing or ruling out gastrointestinal tumors, which require early surgical resection.

[1] *Carney JA, Sheps SG, Go VL, Gordon H. The triad of gastric leiomyosarcoma, functioning extra-adrenal paraganglioma und pulmonary chondroma. N Engl J Med, 1977; 296 (26): 1517–1518.*

Sequences

	Orientation	TI (ms)	TR (ms)	TE (ms)	BW (Hz/Px)	FA (°)	FoV (mm x mm)	Matrix (mm x mm)	No sl.	Slice th. (mm)	Gap	iPAT	TA (s)	
STIR	Tra	130	4510	97	250	133	235 x 320	141 x 256	40	6	0.33	2	30	Mbh
Flash 2D	Tra		196	4.8	200	70	219 x 350	208 x 512	40	5	0.20	Off	40	Mbh
VIBE 3D	Tra		3.4	1.2	455	5	219 x 350	120 x 192	63	1.8		Off	2 x 20	Bh,FS
Flash 3D (angio)	Cor		2.5	1.0	685	15	390 x 390	246 x384	128	1.0		2	19	Bh
VIBE 3D (p.cm)	Tra		4.3	2.1	360	10	241 x 350	236 x 512	72	3		Off	22	Bh,FS

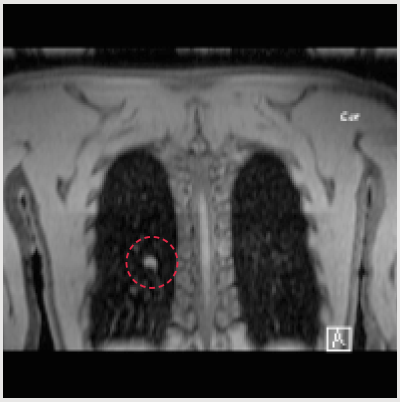

VIBE 3D

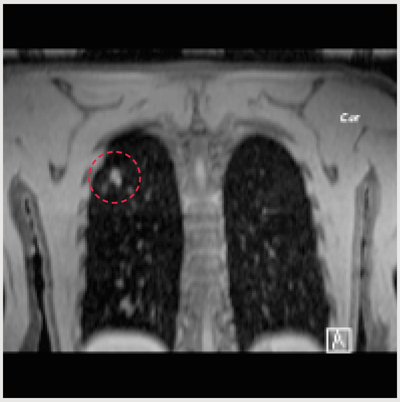

VIBE 3D

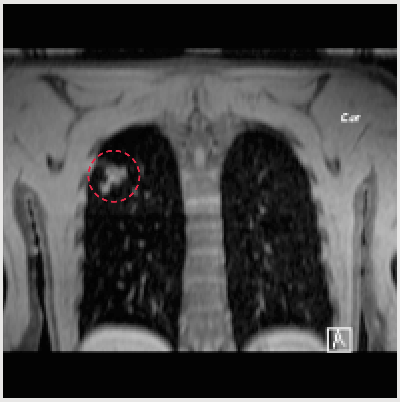

VIBE 3D

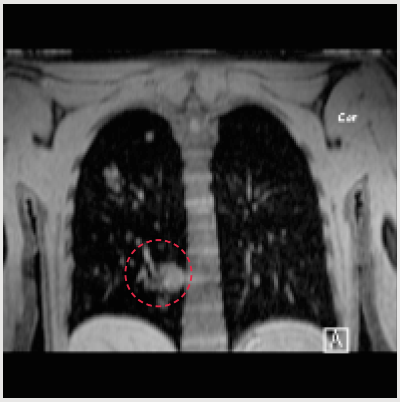

VIBE 3D

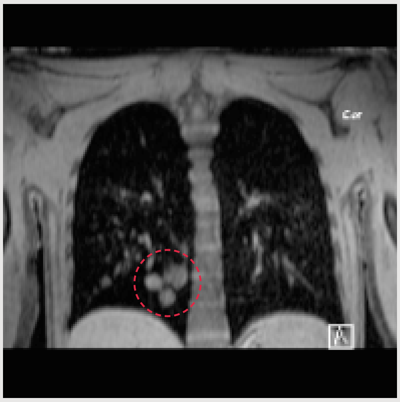

VIBE 3D

VIBE 3D

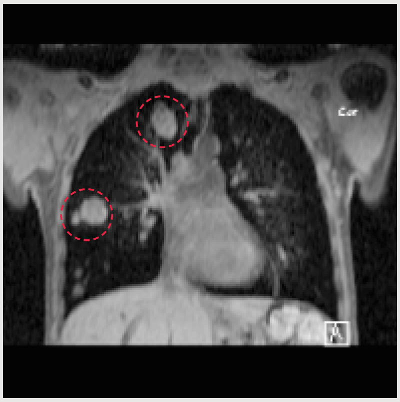

VIBE 3D

VIBE 3D

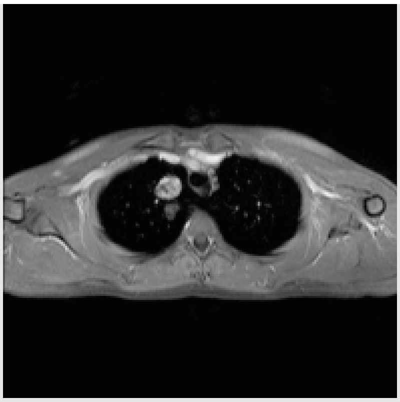

FLASH 2D

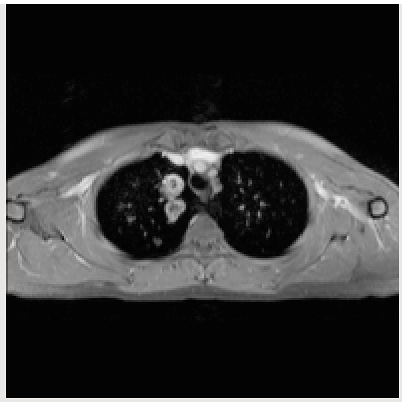

FLASH 2D

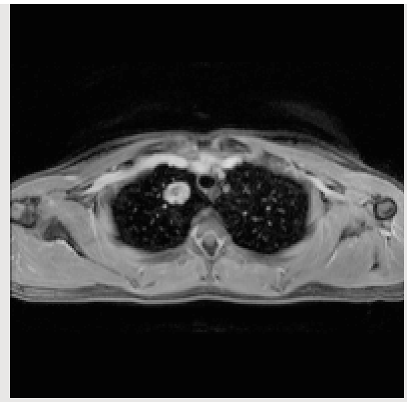

VIBE 3D

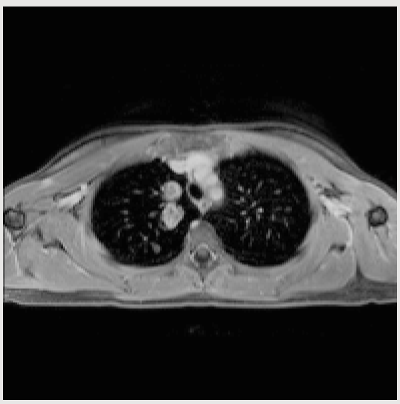

VIBE 3D

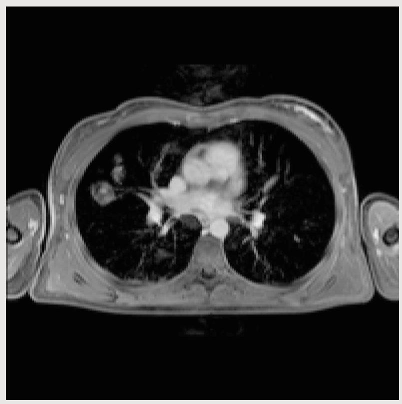

VIBE 3D

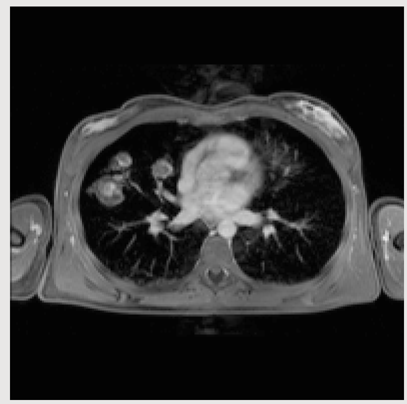

VIBE 3D

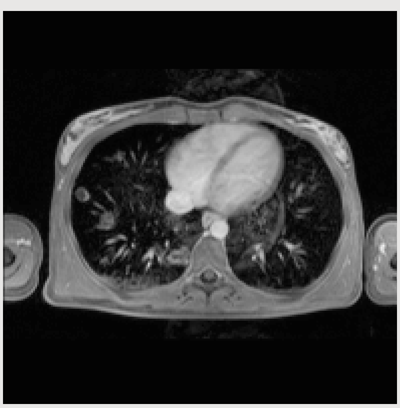

VIBE 3D

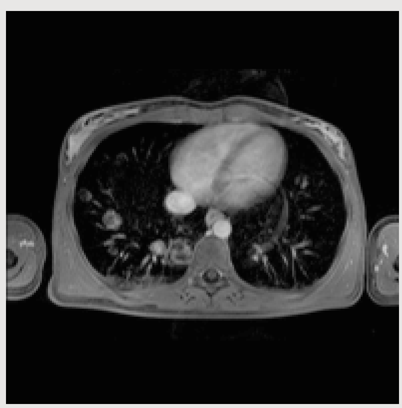

VIBE 3D

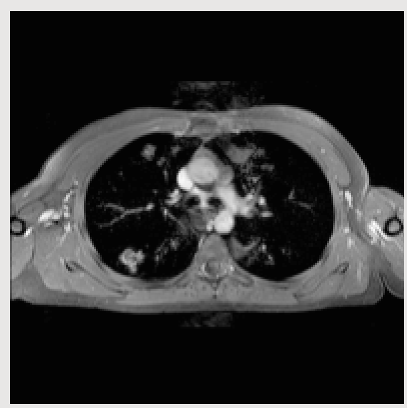

FLASH 2D

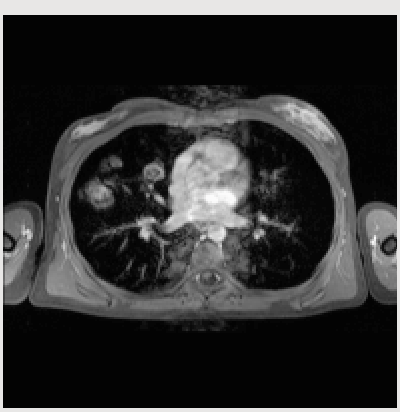

FLASH 2D

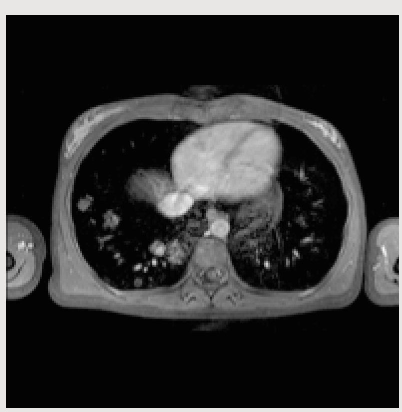

FLASH 2D

MRA MIP view

MRA MIP view

MRA MIP view

MRA MIP view

Case Report: Whole Body MRI

Ulrich Kramer, M.D.
Michael Fenchel, M.D.
Katrin Tomaschko
Heinz-Peter Schlemmer, M.D.

University Hospital Tübingen,
Dept. of Radiology,
Tübingen, Germany

Introduction

Secondary osseous involvement is relatively common in both Hodgkin's disease and non-Hodgkin's lymphoma (up to 16% of cases). As patients with low-grade lymphomas frequently receive high-dose therapy with hematopoietic support, the diagnosis of bone marrow involvement is very important. Today, bone scintigraphy is not widely used in the staging of malignant lymphomas, due to potential false-positive results by skeletal accumulation of the tracer which is not specific to malignancy. Although CT has been used for evaluation of the presence and location of malignant lymphoma, MRI of the bone marrow is a noninvasive and nonradiation imaging method, which can be used to assess stage and prognosis of the disease and to monitor the therapeutic response.

Bone marrow imaging by MRI has proven to be a sensitive technique for determining bone marrow involvement in malignant lymphomas, whereas whole-body MRI has been successfully used to visualize metastatic bone lesions caused by malignant tumors.

Patient History

52 year old male patient with known non-Hodgkin's lymphoma involving lungs, liver, spleen and gastrointestinal structures. MRI was requested in addition to conventional contrast-enhanced whole-body CT for precise tumor staging and follow-up.

Examination

Examination was performed on a 1.5T Siemens **MAGNETOM Avanto** scanner using head-, neck-, spine-, peripheral angiography – and two Body Matrix coils.

Five segments were planned for complete cranio-caudal coverage with overlap between two adjacent segments of at least 40 mm. Segment one encompassed head and upper thorax, segment two lower thorax and abdomen, segment three pelvis, segment four upper leg and segment five lower leg.

Firstly, STIR sequences using parallel imaging (GRAPPA, PAT factor 2) were performed in coronal orientation for all five segments. Field of view (FoV) was 480 mm in each case, yielding 2020 mm head to feet coverage.

Secondly, brain, neck, thorax, abdomen and pelvis were examined with T2-weighted sequences as well as precontrast T1-weighted sequences in axial orientation. Postcontrast T1-weighted fat suppressed images were acquired after injection of 0.1 mmol Gadolinium-DTPA (Magnevist, Schering, Germany).

T2-weighted imaging was performed using a fluid attenuated inversion recovery sequence (FLAIR) for the brain, STIR sequences for the neck, thorax and pelvis and a TSE sequence with fat saturation for the abdomen. While thoracic images were acquired in breath-hold technique, the abdomen was examined using navigator triggered sequences. Precontrast T1-weighted MRI was performed using a SE sequence for the brain and a FLASH 2D with fat saturation for the abdomen. The thorax was imaged using a PD-weighted volumetric interpolated 3-dimensional breath-hold (VIBE) sequence with fat saturation. After contrast application, coronal and axial T1-weighted SE sequences for brain, T1-weighted FLASH 2D with fat saturation for the neck, abdomen and pelvis and a T1-weighted fat saturated VIBE for the thorax were acquired. 40 mg of n-butyl-scopolamide (Buscopan, Boehringer, Germany) were administered intravenously just before abdominal MRI to suppress bowel peristalsis.

Findings

1. Head/neck: NAD, particularly no tumor suspicious lymph nodes were detected

2. Thorax: lymph node involvement next to the left internal mammarian artery, pulmonary nodules in left (diameter: 34 mm) and right lung (diameter: 44 mm); extramedullary involvement left to thoracic vertebrae 10-12.

3. Abdomen/pelvis: splenomegaly, multiple tumor suspicious lesions in liver and spleen, tumor suspicious bone marrow changes, especially in ilium and sacrum.

Discussion

MRI has high sensitivity for visualizing bone marrow involvement in malignant diseases, particularly with STIR or fat-suppressed T2-weighted MR images providing high contrast between tumor and uninvolved bone marrow. Moreover, MRI allows to demonstrate extramedullary tumor involvement in lung, abdominal and pelvic organs as well as soft tissue. Whole-body MRI is consequently an effective method for a comprehensive evaluation of both bone marrow and extramedullary involvement of the entire body in patients with non-Hodgkin's lymphoma.

Sequences

	Orientation	*TI (ms)*	*TR (ms)*	*TE (ms)*	*BW (Hz/Px)*	*FA (°)*	*FoV (mm x mm)*	*Resolution (mm x mm x mm)*	*No slices*	*Slice th.*	*Gap*	*iPAT*	*TA*	
STIR (head/thorax)	*Cor*	*150*	*9760*	*87*	*305*	*150*	*480*	*1.8 x 1.3 x 5.0*	*30*	*5 mm*	*0.20*	*2*	*2:36 min*	
STIR (thorax/abd)	*Cor*	*150*	*5800*	*87*	*305*	*150*	*480*	*1.8 x 1.3 x 5.0*	*38*	*5 mm*	*0.20*	*2*	*3:06 min*	
STIR (pelvis/upper leg)	*Cor*	*150*	*8540*	*87*	*305*	*150*	*480*	*1.8 x 1.3 x 5.0*	*30*	*5 mm*	*0.20*	*2*	*2:17 min*	
STIR (up.leg/ knee)	*Cor*	*150*	*7020*	*87*	*305*	*150*	*480*	*1.8 x 1.3 x 5.0*	*25*	*5 mm*	*0.20*	*2*	*1:52 min*	
STIR (knee/ lower leg)	*Cor*	*150*	*8670*	*87*	*305*	*150*	*480*	*1.8 x 1.3 x 5.0*	*25*	*5 mm*	*0.20*	*2*	*2:02 min*	
Flair (brain)	*Tra*	*2500*	*8510*	*108*	*130*	*150*	*230*	*1.2 x 0.9 x 4.0*	*30*	*4 mm*	*0.10*	*Off*	*2:40 min*	
T1 se (brain)	*Tra*		*500*	*8*	*130*	*90*	*230*	*0.9 x 0.9 x 4.0*	*30*	*4 mm*	*0.10*	*Off*	*2:48 min*	
STIR (neck)	*Tra*	*150*	*6180*	*59*	*130*	*150*	*220*	*1.2 x 0.9 x 5.0*	*40*	*5 mm*	*0.20*	*2*	*2:17 min*	
STIR (thorax)	*Tra*	*150*	*4480*	*100*	*250*	*146*	*380*	*1.8 x 1.2 x 6.0*	*30*	*6 mm*	*0.33*	*2*	*0:48 min*	*mbh*
VIBE 3D (thorax)	*Tra*		*3.37*	*1.21*	*455*	*5*	*380*	*2.0 x 2.0 x 2.0*	*72/slab*	*2 mm*		*Off*	*0:20 min x2*	*Bh, FS*
T2 tse fs (abdomen)	*Tra*		*6859*	*95*	*300*	*150*	*380*	*1.6 x 1.2 x 6.0*	*40*	*6 mm*	*0.33*	*2*	*1:46 min*	*trigger, FS*
Flash 2D fs (abdomen)	*Tra*		*242*	*4.10*	*140*	*70*	*380*	*2.1 x 1.5 x 6.0*	*40*	*6 mm*	*0.33*	*2*	*0:59 min*	*mbh, FS*
STIR (pelvis)	*Tra*	*150*	*7100*	*70.00*	*130*	*150*	*360*	*1.3 x 1.0 x 4.0*	*40*	*4 mm*	*0.25*	*2*	*4:31 min*	
Flash 2D fs (pelvis)	*Tra*		*216*	*4.10*	*140*	*70*	*360*	*2.1 x 1.5 x 4.0*	*40*	*4 mm*	*0.25*	*2*	*0:57 min*	*FS*
Flash 2D fs (abdomen)	*Tra*		*242*	*4.10*	*140*	*70*	*380*	*2.1 x 1.5 x 6.0*	*40*	*6 mm*	*0.33*	*2*	*0:57 min*	*FS*
VIBE 3D fs (thorax)	*Tra*		*3.37*	*1.21*	*460*	*20*	*380*	*2.0 x 2.0 x 2.0*	*72/slab*	*2 mm*		*Off*	*0:20 min x 2*	*FS*
Flash 2D fs (neck)	*Tra*		*554*	*4.10*	*150*	*70*	*220*	*1.1 x 0.8 x 5.0*	*40*	*5 mm*	*0.20*	*2*	*1:15 min*	*FS*
T1 se (brain)	*Tra*		*500*	*8*	*130*	*90*	*230*	*0.9 x 0.9 x 4.0*	*30*	*4 mm*	*0.10*	*Off*	*3:48 min*	
T1 se (brain)	*Tra*		*500*	*8*	*130*	*90*	*230*	*0.9 x 0.9 x 4.0*	*40*	*4 mm*	*0.10*	*Off*	*4:14 min*	

T2 TSE fs

VIBE 3D

FLASH 2D fs

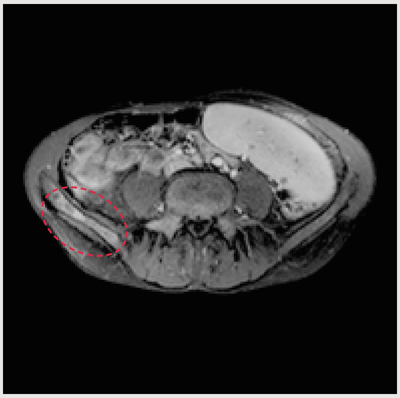

FLASH 2D fs

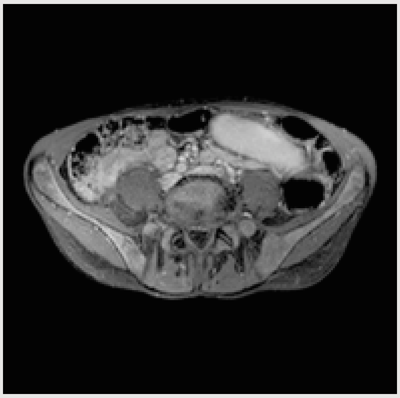

FLASH 2D fs

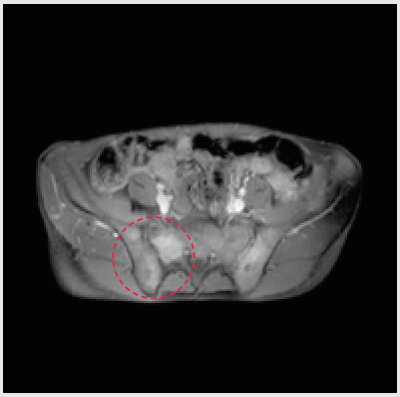

FLASH 2D fs

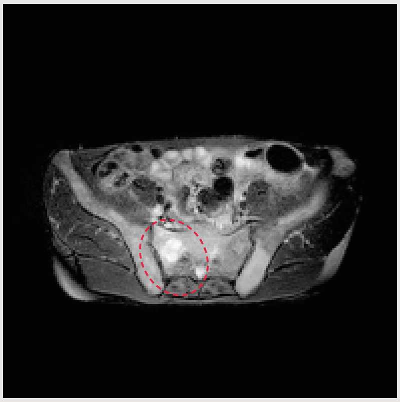

T2 TSE fs

STIR

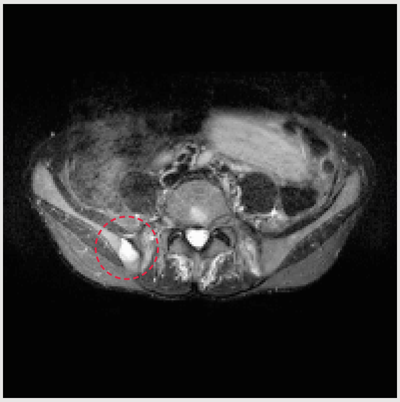

STIR

STIR

STIR

STIR

STIR

STIR

STIR

STIR

STIR

STIR

STIR

STIR

STIR

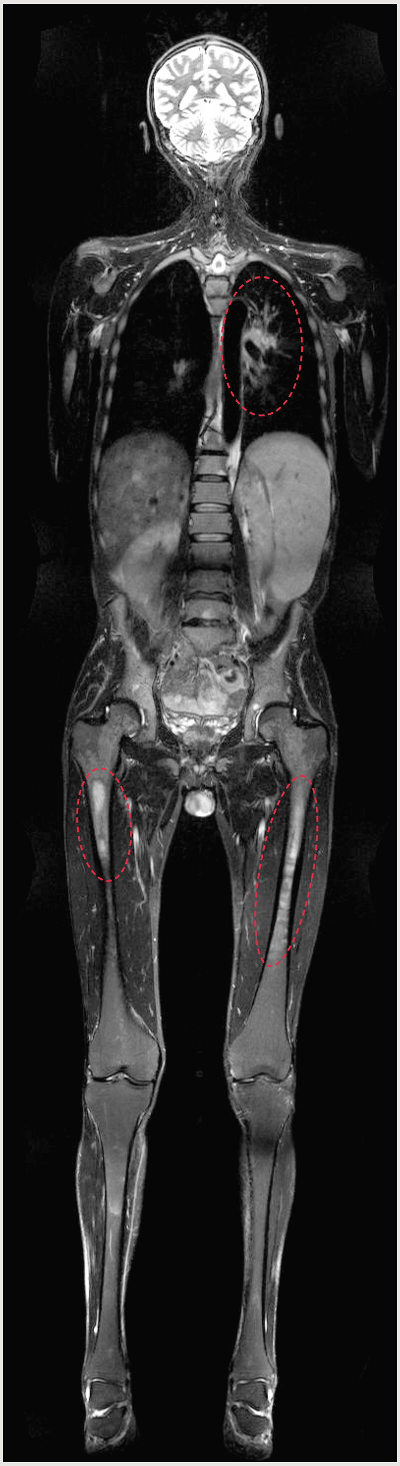

STIR

STIR

STIR

STIR

STIR

STIR

STIR

STIR

STIR

Case Report: MRI of the Lower Extremities

Michael Fenchel, M.D.
Ulrich Kramer, M.D.
Katrin Tomaschko
Heinz-Peter Schlemmer, M.D.

University Hospital Tübingen,
Dept. of Radiology,
Tübingen, Germany

Patient History

MRI was performed on a 10 year old male patient who already had a previous MR examination of the ankle several days before. Due to image findings, suspicious for an osteosarcoma, a whole body scintigraphy was conducted which shows enhancement of the proximal tibia, the knee and the femur. No abnormalities were detected on plain x-ray films of the distal tibia.

For additional information, MR images of the pelvis, the upper and lower leg were acquired to determine tumor location as well as tumor spread.

Examination

Examination was performed on a 1.5T Siemens **MAGNETOM Avanto** scanner. The child was positioned feet first supine in the magnet. The Pelvis and the legs of the patient were covered with a Body Matrix and the Peripheral Angiography Matrix coil. Four spine elements were also used on each station to increase the signal.

T2-weighted STIR sequences and T1-weighted spin echo sequences were measured in coronal and axial slice orientation on two stations with sufficient overlap. T1-weighted sequences were repeated with fat saturation after the injection of Gadolinium-DTPA (0.1 mmol/kg body weight). Subsequently, coronal images were composed for a “whole-leg-image” for improved visualization of the tumor.

Findings

Extensive lymph node packages were detected in the inguinal and iliac region on the left side. Singular lymph nodes measure up to 3.5 x 3.0 cm. Marked signal enhancement on STIR MR images and post contrast images secondary to inflammatory signs of the surrounding tissues. In the distal femur diaphysis (left side) an intramedullary signal enhancement (size 4.0 cm) can be observed, without affection of the cortical bone. No sign of periostal involvement.

Additional signal increase on STIR MR images and contrast enhancement at the level of the tibial plateau.

In the distal femoral metaphysis (right side), an additional tumorous lesion was detected which crosses the epiphyseal border.

Extensive tumorous involvement of the tibila plateaus on both sides, the right distal femur and the left distal femoral diaphysis. Widespread lymphoma of the left inguinal and iliac region. Due to serological data, an inflammatory disease can be ruled out. Secondary to the multifocal affection there is evidence of a lymphoma in conjunction with an osteosarcoma.

Discussion

The large field-of-view of the MAGNETOM Avanto was helpful for evaluating all tumor-involved regions as compared to initial MR imaging restricted to the lower legs.

Novel image post-processing techniques using the “Composing” Tab Card allow for an improved visualization of all body regions.

Sequences

	Orientation	*TI (ms)*	*TR (ms)*	*TE (ms)*	*BW (Hz/Px)*	*FA (°)*	*FoV (mm x mm)*	*Matrix (mm x mm)*	*No sl.*	*Slice th. (mm)*	*iPAT*	*TA (min)*	
STIR (pelvis/upper leg)	*Cor*	*150*	*8540*	*87*	*305*	*150*	*480 x 480*	*269 x 384*	*28*	*5*	*2*	*2:20*	
STIR (knee/lower leg)	*Cor*	*150*	*4580*	*87*	*305*	*150*	*480 x 480*	*269 x 384*	*30*	*5*	*2*	*2:18*	
STIR	*Tra*	*150*	*7620*	*69*	*130*	*150*	*227 x 351*	*133 x 256*	*50*	*6*	*2*	*2:00*	
SE	*Tra*		*546*	*13*	*150*	*90*	*219 x 350*	*129 x 256*	*50*	*6*	*2*	*2:00*	
SE p.KM	*Tra*		*687*	*13*	*150*	*90*	*219 x 350*	*112 x 256*	*50*	*6*	*2*	*3:00*	*FS*
SE p.KM (pelvis/upper leg)	*Cor*		*568*	*13*	*150*	*90*	*480 x 480*	*179 x 256*	*28*	*5*	*2*	*3:00*	*FS*
SE p.KM (knee/lower leg)	*Cor*		*609*	*13*	*150*	*90*	*480 x 480*	*179 x 256*	*30*	*5*	*2*	*3:10*	*FS*

STIR

STIR

STIR

STIR

STIR

STIR

Case Report: MR-Urography

Ulrich Kramer, M.D.
Michael Fenchel, M.D.
Katrin Tomaschko
Heinz-Peter Schlemmer, M.D.

University Hospital Tübingen,
Dept. of Radiology,
Tübingen, Germany

Patient History

A 68 year old male patient status post radical prostatectomy and urinary bladder resection because of urothelial carcinoma. Construction of a neo-bladder using the ileum. The patient is now presenting with urinary retention to the left kidney. Renal function was assessed by scintigraphy: left/right kidney 15.5%/84.5%.

Examination

MR images were acquired on a 1.5T Siemens **MAGNETOM Avanto** scanner using two standard Body Matrix coils. The patient was placed in supine position, 40 mg of n-butyl-scopolamide (Buscopan, Boehringer, Germany) were administered intravenously to suppress bowel peristalsis. Coronal HASTE images provide initial information about the abdominal anatomy. The urinary bladder was examined using an axial T2-weighted TSE sequence. Subsequently, the table was moved and T1- and T2-weighted axial images covering the kidneys were acquired using breath-hold and navigator triggering techniques. For the urography without contrast agent, we used a heavily T2-weighted 3D sequence with navigator triggering. Contrast media was administered to analyze the perfusion of the kidneys. Contrast enhanced urography was performed after 25 minutes, using a T1-weighted sequence with fat saturation.

Findings

MRI was performed to assess the whole urinary tract including kidneys and the ileum-bladder and to exclude recurrence of the tumor.

No tumor was detected. Distal ureter stenosis secondary to scar tissue was treated by dilatation.

Discussion

Heavily T2-weighted urography without contrast agent is feasible yielding state-of-the-art image quality. In this case a contrast enhanced urography was performed, as the patient had received Gadolinium for the assessment of renal perfusion, despite excellent diagnostic quality of precontrast urographic images.

Sequences

	Orientation	*TR (ms)*	*TE (ms)*	*BW (Hz/Px)*	*FA (°)*	*FoV (mm x mm)*	*Matrix (mm x mm)*	*No sl.*	*Slice th. (mm)*	*Gap*	*iPAT*	*TA (s)*	
HASTE (abdomen)	*Cor*	*900*	*118*	*490*	*106*	*500 x 500*	*412 x 512*	*40*	*5*	*0.20*	*Off*	*0:30*	*Mbh*
T2 TSE (bladder)	*Tra*	*5700*	*130*	*130*	*137*	*321 x 400*	*278 x 384*	*40*	*4*	*0.25*	*2*	*3:10*	
Flash 2D (kidneys)	*Tra*	*187*	*4.1*	*140*	*70*	*375 x 400*	*167 x 256*	*36*	*5*	*0.20*	*2*	*0:36*	*Mbh*
T2 TSE FS (kidneys)	*Tra*	*3890*	*96*	*300*	*150*	*400 x 400*	*240 x 320*	*36*	*5*	*0.20*	*2*	*1:46*	*Trigger*
T2 TSE (kidneys)	*Tra*	*3100*	*100*	*260*	*150*	*369 x 400*	*284 x 512*	*36*	*5*	*0.20*	*Off*	*0:40*	*Mbh*
TrueFISP (abdomen)	*Tra*	*3.3*	*1.4*	*750*	*60*	*400 x 400*	*220 x 256*	*40*	*6*	*0.33*	*Off*	*0:30*	*Mbh*
T2 TSE 3D (urography)	*Cor*	*3713*	*678*	*260*	*180*	*450 x 450*	*380 x 384*	*40*	*1.5*		*2*	*3:42*	*Trigger*
T1 SE FS (bladder)	*Cor, tra,sag*	*662*	*13*	*150*	*90*	*280 x 280*	*179 x 256*	*30*	*3*	*0.33*	*2*	*3:20*	*FS*
Flash 2D FS (abdomen)	*Tra*	*107*	*2.9*	*210*	*70*	*375 x 400*	*336 x 512*	*60*	*5*	*0.20*	*Off*	*1:30*	*Mbh, FS*
Flash 3D (urography)	*Cor*	*3.1*	*1.1*	*425*	*25*	*500 x 500*	*308 x 512*	*80*	*1.5*		*2*	*0:18*	*Bh*

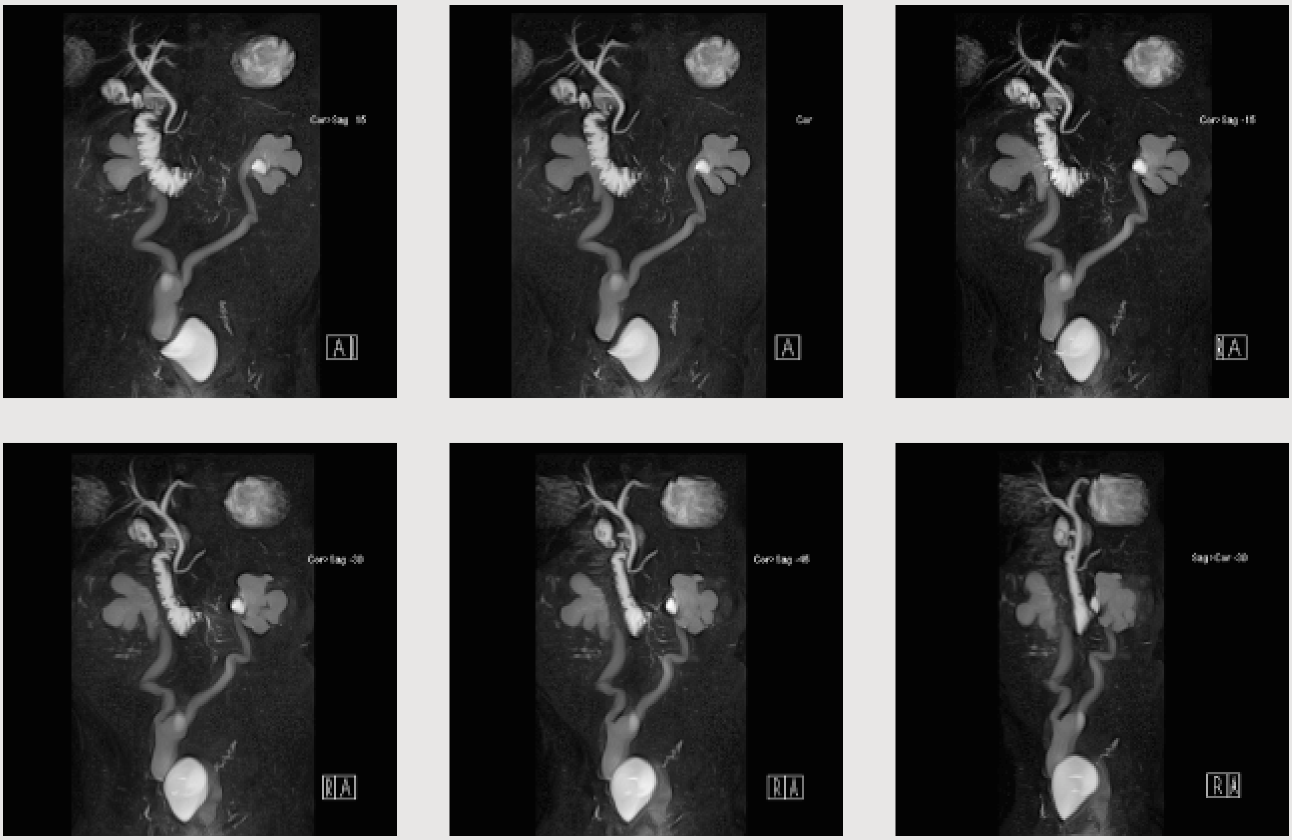

T2-weighted 3D TSE, Maximum Intensity Projection (MIP) images.

Case Report: Pediatric MRI of the Hepatobiliary System

Michael Fenchel, M.D.
Ulrich Kramer, M.D.
Katrin Tomaschko
Heinz-Peter Schlemmer, M.D.

University Hospital Tübingen,
Dept. of Radiology,
Tübingen, Germany

Patient History

4 months old male patient with a history of choleocysto- and choleodocholithiases; no concrements were detected on ultrasound.

Examination

Examination was performed on a 1.5T Siemens **MAGNETOM Avanto** scanner using a standard 8 channel head coil. After the child was sedated and 5 mg of butyl-scopolamide (Buscopan, Boehringer, Germany) were administered to suppress bowel peristalsis, T2- and T1-weighted images were obtained to get an anatomical overview. The T1-weighted sequence was acquired with four repetitions to decrease respiratory movement; the T2-weighted sequences were measured during free breathing using PACE (Prospective Acquisition CorrEction) navigator triggering. After localizing the bile ducts, a heavily T2-weighted coronal TSE 3D sequence was measured with PACE navigator technique. T2-weighted coronal TSE 3D images were post-processed using a maximum intensity projection (MIP) algorithm.

Findings

Discrete dilatation of intrahepatic biliary ducts (up to 6 mm). Irregular shape of the ductus choledochus. Evidence of concrements in the gall bladder as well as prepapillary concrements in the hepatobiliary duct (size 3 and 1.2 mm). Normal appearance of other abdominal organs and structures. There is no evidence of a significant cholangitis.

Discussion

Assessment of the pancreato-biliary system without contrast agent is a valuable tool in pediatric and adult patients. The use of PACE navigator triggering and parallel imaging techniques is particularly promising because heavily T2-weighted 3D data sets can be acquired within reasonable imaging times depicting the anatomy of the pancreato-biliary system in great detail.

The safety of imaging (fetuses, infants) has not been established.

Sequences

	Orientation	*TR (ms)*	*TE (ms)*	*BW (Hz/Px)*	*FA (°)*	*FoV (mm x mm)*	*Matrix (mm x mm)*	*No sl.*	*Slice th. (mm)*	*iPAT*	*TA (min)*	
HASTE	*Cor*	*1100*	*119*	*490*	*120*	*175 x 200*	*179 x 256*	*22*	*4*	*2*	*0:29*	
T1 TSE	*Tra*	*465*	*16*	*250*	*150*	*129 x 180*	*294 x 512*	*30*	*4*	*2*	*4:30*	
T2 TSE FS	*Tra*	*3010*	*71*	*300*	*150*	*125 x 196*	*153 x 320*	*30*	*4*	*2*	*3:00*	*FS*
T2 TSE FS	*Cor*	*2995*	*71*	*300*	*150*	*180 x 200*	*216 x 320*	*22*	*4*	*2*	*3:10*	*FS*
T2 TSE 3D	*Cor*	*2767*	*683*	*260*	*180*	*200 x 200*	*380 x 384*	*44*	*1.5*	*2*	*4:34*	

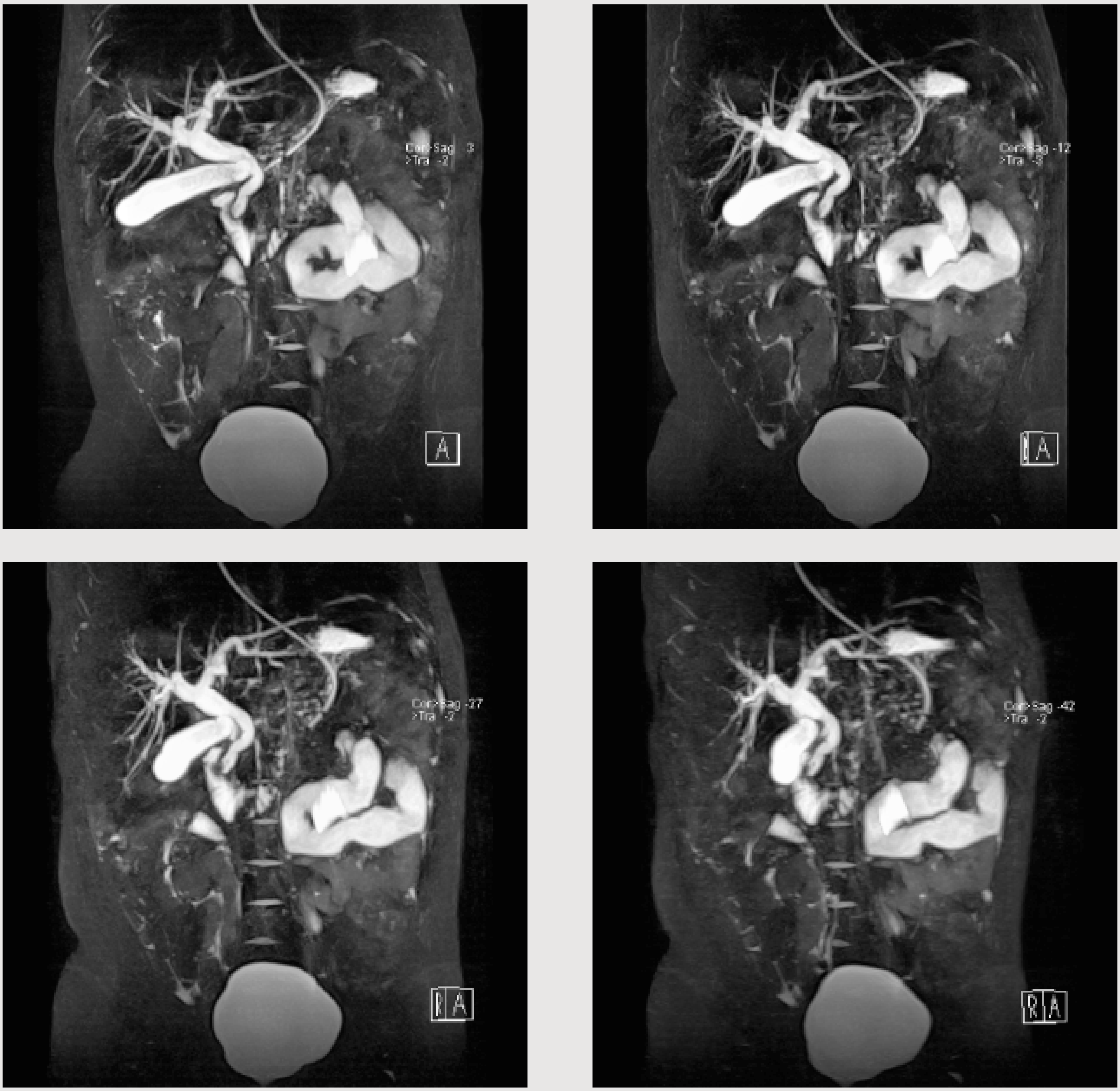

T2-weighted 3D TSE.

The safety of imaging (fetuses, infants) has not been established.

Case Report: Whole Body MRA

Ulrich Kramer, M.D.
Michael Fenchel, M.D.
Katrin Tomaschko
Stephan Miller

University Hospital Tübingen,
Dept. of Radiology,
Tübingen, Germany

Introduction

The early detection of atherosclerotic vascular lesions is very important for diagnostic and interventional purposes. Magnetic resonance angiography (MRA) has increasingly gained acceptance as a valid alternative to conventional digital subtraction angiography for many vascular regions. The systemic distribution of atherosclerotic manifestations requires the use of techniques which can assess the vascular system as exhaustively as possible. The recent introduction of whole-body MR scanners with surface coil technology raises the possibility of whole-body MRA examinations providing information of the patient's complete arterial vasculature.

Patient History

Whole body MRA was performed on a 45 year old male patient with suspected peripheral arterial occlusive disease (Fontaine 2b). According to patient history and clinical findings, arterial obstruction is suspected at the level of the upper leg.

Prior angiographic examinations were performed in 1992 and March of 2004. However, due to atherosclerotic occlusions of the pelvic arteries, only an intravenous DSA could be performed.

MR images should be acquired to assess the vascular status of the complete arterial vasculature of the body.

Examination

Examination was performed on a 1.5T Siemens **MAGNETOM Avanto** scanner using standard Head-, Neck-, Spine-, Peripheral Angio- and two Body Matrix coils.

The patient was placed in supine position with pads under each knee to reduce the venous backflow. Venous access was established on the right cubital vein to avoid overlapping with the left subclavian artery in the maximum intensity projection (MIP).

Four angiographic stations were acquired to obtain whole-body coverage. Station I included cranial and thoracic vessels, station II thoracic, abdominal and pelvic vessels, station III vessels of the upper leg and station IV vessels of the lower leg. Field of view (FoV) was 500 mm for each station and overlap between two stations was at least 40 mm.

After acquisition of localizer images in all four regions, a phase-contrast vessel scout was obtained for each station.

A test bolus (2 ml Magnevist) was injected to determine contrast circulation time according to the following formula: [circulation time – time to k-space center + 4 seconds]. Subsequently, a multislab time-of-flight (TOF) sequence (TR = 36 ms, TE = 7.15 ms, FoV = 220 mm, Flip = 30°, BW = 73Hz/Px, slice thickness = 0.80, gap = -34%, voxel size: 0.8 mm x 0.6 mm x 0.8 mm) employing a TONE pulse was used to depict the cranial arterial vessels with sufficient spatial resolution.

Precontrast and postcontrast images of all regions were acquired using an angiographic FLASH 3D sequence in coronal orientation (see table for sequence details).

Findings

Normal anatomy of intracranial arteries as well as common carotid arteries and internal carotid arteries. There is a low grade stenosis of the external carotid arteries. Normal depiction of thoracic, abdominal aorta and great thoracic vessels.

Both kidneys are supplied by two renal arteries; one renal artery of the right kidney which exhibits a hemodynamically relevant stenosis.

An occlusion of the left common iliac artery as well as a high grade stenosis of the right common iliac artery can be found. Complete occlusion of the distal superficial femoral arteries on both sides with collaterals to normal perfused lower leg arteries.

Discussion

The presented technique is very promising for a comprehensive staging of vascular involvement of systemic atherosclerotic disease. Novel scanner and coil technology enable whole-body MRA examinations without patient repositioning while providing high SNR in short measuring times.


Cor>Tra 5
>Sag -0
A

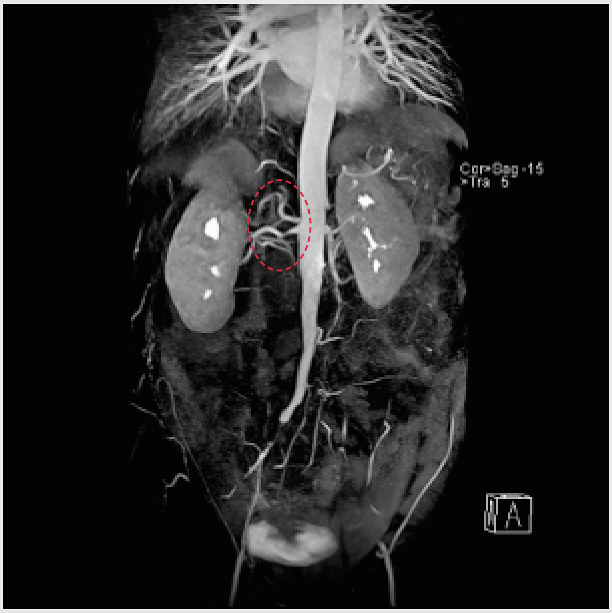
Cor>Sag -15
>Tra 5
A


Cor>Tra -6
>Sag -0
A


Cor>Tra -1
>Sag -0
A

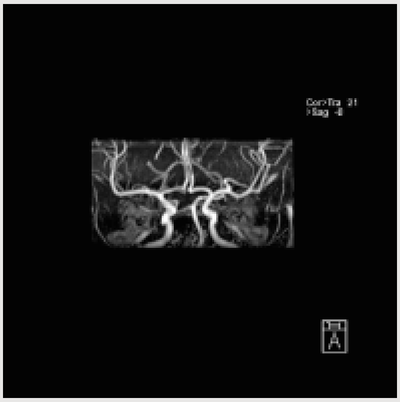

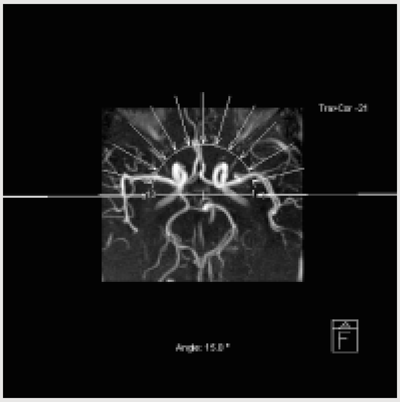

	Orientation	TR (ms)	TE (ms)	BW (Hz/Px)	FA (°)	FoV (mm x mm)	Matrix (mm x mm)	No sl.	Slice th. (mm)	iPAT	TA (min)	
Flash 3D (head/thorax)	Cor	2.85	1.68	650	25	344 x 500	264 x 512	88	1.6	2	0:17	Bh
Flash 3D (abdomen)	Cor	3.11	1.14	420	25	375 x 500	230 x 512	80	1.5	2	0:13	Bh
Flash 3D (upper leg)	Cor	3.46	1.21	360	25	375 x 500	230 x 512	64	1.5	2	0:12	
Flash 3D (lower leg)	Cor	3.46	1.21	360	25	375 x 500	230 x 512	80	1.3	Off	0:26	
TOF (brain vessels)	Tra	36	7.15	73	30	180 x 240	202 x 384	84	0.8	Off	5:30	

M-Z848-2-7600

Proven Outcomes in Magnetic Resonance. MAGNETOM® Avanto, the world's first Tim™ system, takes sound to a new, and very low level. While still delivering powerful gradient performance unmatched by anything else – and essential for today's most demanding applications. MAGNETOM Avanto's AudioComfort enables an acoustic noise reduction of up to 30 dB(A).

MAGNETOM Avanto. It looks different. It sounds different. It works differently, too. To learn more, visit us at www.siemens.com/Tim.

Siemens **Medical Solutions** that help

SIEMENS
medical

All You Want to Know about FatSat

David Purdy, Ph.D.

MR R&D
Research & Collaborations,
USA

Quick FatSat

What is Quick FatSat and why do we need it ?

Fat and water saturation pulses take so much time compared to the rest of a gradient echo sequence that acquisition times become nearly as long as the corresponding spin echo sequence. In standard saturation mode, saturation pulses are applied before every phase-encoding step of every slice. The quick saturation mode provides a significant reduction in imaging time by using fewer saturation pulses while maintaining a reasonable level of fat or water suppression. This technique is only available for the gradient echo sequence.

How is Quick FatSat used with *syngo*?

Choose two or more slices to ensure that the Saturation mode selection is active in the Saturation subcard of the Geometry card. Select Saturation mode = Quick. Then select Q-fat sat or Q-water sat.

Quality versus imaging time

In quick saturation mode, gradient echo slices are acquired with varying degrees of saturation. The "strong" option gives more slices with good fat saturation in a relatively short imaging time. Even shorter acquisition times are available with the "weak" option, which also gives some slices with good fat saturation, but permits more of the slices to have poorer saturation. This allows the user to adjust the trade-off between imaging time and fat saturation quality when speed is essential, often for breath-hold imaging.

Quick FatSat with 2D Multislice

Since the effect of a saturation pulse does not disappear immediately, and since the GRE sequence acquires data rapidly, one Fourier line from several slices can be acquired after a single saturation pulse. Naturally, the first slice acquired following the saturation pulse will show better saturation than the last, so the user is allowed some control over how many slices are acquired before the next saturation.

For strong Quick fat sat mode, the system acquires as many different slices as possible between FatSat pulses, provided that the time between saturation pulses does not exceed about 50 ms. This amounts to roughly four slices between saturation pulses, greatly increasing the time efficiency of the sequence. For the "weak" fat sat mode, the time between saturation pulses does not exceed about 75 ms, further increasing time efficiency at the cost of poorer fat suppression for a few of the slices.

You can obtain the maximum number of slices per FatSat pulse if you increase the number of slices to the final value, rather than decreasing the number.

If only two slices are acquired, there are only two slices between saturation pulses, and there is no difference between "strong" and "weak" quick saturation modes. The same will usually be true for three and four slice protocols. The gradient echo sequence does not change the FatSat flip angle to create brighter or darker fat.

If only one slice is acquired, the saturation pulse must be applied for each phase encoding, so there is no difference between quick saturation mode and standard mode.

Quick FatSat with 2D Sequential Slice

The saturation pulse must be applied for each phase encoding, so there is no difference between quick saturation mode and standard mode.

Quick FatSat with the 3D GRE Sequence

For a single slab (or multiple, sequential slabs), the quick and standard saturation modes are identical. For multiple interleaved slabs, the quick mode works as described above for interleaved slices. For 3D, users should select the "weak" Q-fat sat mode to avoid a system problem with the "strong" mode. For a faster acquisition with good fat suppression, a water excitation pulse should be considered.

Quick FatSat: Some Examples

A concrete example is helpful for explaining how Quick FatSat works. Here is my test case :

I used the gradient echo sequence on a MAGNETOM Symphony Quantum, regular gradient mode, regular RF mode, 260 Hz/pixel bandwidth, one segment, minimum TE, and minimum TR. For acquisition time measurements, I used a 256 x 256 matrix.

To describe what is happening, I need to define a couple of words. I will call that part of the sequence that excites the slice, phase-encodes it, and reads out the data the "imaging module." The duration of the imaging module is the same as the minimum TR of the sequence (without saturation pulses) when one slice is imaged. This is a few milliseconds longer than TE. For my test case, TE is 3.76 ms and the imaging module takes 7.7 ms.

I will call the FatSat RF pulse and the following spoiler gradient the "FatSat module." For the GRE sequence, the FatSat or Water sat module takes about 20 milliseconds.

The operation of the quick saturation mode is governed by several concepts or rules.

Rules:

1. The effectiveness of the FatSat pulse decays over time: 30 ms after the pulse, the fat suppression is only "fair"; 55 ms after the pulse, the suppression is just adequate. For the standard FatSat technique, only one imaging module is placed after each FatSat module, so that the strongest saturation is obtained. However, additional imaging modules (e.g., slices) may be placed after the first. This reduces imaging time. Images reconstructed from these later imaging modules will have poorer fat saturation.

2. The time between the imaging modules for a particular slice is TR. To avoid serious artifacts, the TR for all 256 Fourier lines must be the same.

3. To maintain the same clinical contrast for every slice, the TR of each slice should be the same.

4. To avoid artifacts, the time between the FatSat module and the imaging module for a particular slice should be the same for all 256 Fourier lines.

5. It is not necessary for the time between FatSat pulses to be constant.

These considerations lead naturally to the Quick saturation method: more than one imaging module may be placed after a FatSat module. This technique was originated by Dr. Paul Finn (U.S. patent 5.633.586). The sequence diagrams are rather different for one slice, a few slices, and many slices, and I will treat these separately.

Quick Sat – Small number of slices

The advantage of Quick saturation is most easily diagrammed for two slices.

Figure 1 shows a two-slice interleaved multislice sequence with standard FatSat:

Each imaging module acquires one Fourier line, and each is directly preceded by a FatSat module. Each Fourier line has good fat suppression, and the two images do also. TR is the sum of the durations of two FatSat and two imaging modules (20 + 20 + 7.7 + 7.7 = 55.4 ms). The time between the centers of the FatSat modules is (20 + 7.7 = 27.7 ms). The desirable short acquisition time of the GRE sequence is lost when FatSat is added in this manner – the FatSat module takes up 20/27.7 = 72% of the overall imaging time.

The Quick saturation mode saves time by inserting the imaging modules for slice 2 immediately after the modules for slice 1 (Figure 2). This eliminates half (256) of the FatSat modules from the acquisition. The fat suppression for slice 2 is not as good as that for slice 1, but it is acceptable as long as not too much time has elapsed between the FatSat pulse and the second slice module. The *syngo* Quick sat mode guarantees this.

Standard saturation, 2 slices

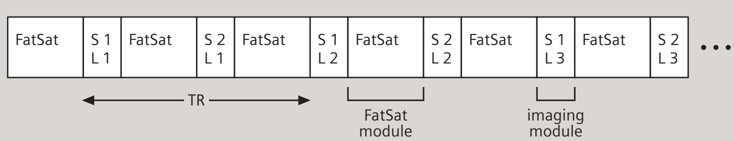

Figure 1 *Each imaging module is labeled with the spatial slice position (S) and the Fourier line number (L). The horizontal axis is time. The 2 slice, 256 line acquisition has 512 FatSat modules.*

QuickSat, 2 slices, "strong" or "weak"

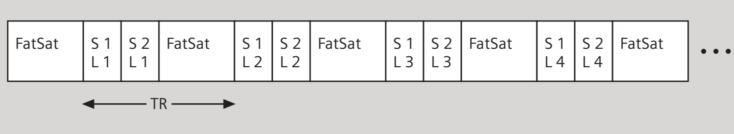

Figure 2 *Compared to the standard saturation mode in Figure 1, the FatSat module now only takes up 56% of the total imaging time. The time between FatSat modules (center-to-center or end-to-end) is labeled "F-F time."*

TR has been reduced to one FatSat module and two imaging modules (20 + 7.7 + 7.7 = 35.4 ms), and the total imaging time (256 x TR) has been reduced from 14.2 seconds in standard mode to 9.1 seconds in Quick sat mode, a time saving of 36%.

The fat saturation of the second slice in Figure 2 is still fairly good, so more imaging modules (slices) may be added between the FatSat pulses. Since each additional slice has poorer saturation, we cannot insert too many slices between FatSat modules. The user is given some control over the tradeoff between speed and FatSat quality. In "strong" mode, the FatSat-to-FatSat time (measured from the pulse centers) will not exceed about 50 milliseconds (four slices for our test case). In "weak" mode, the time limit is about 75 ms (seven slices for our test case). One measure of the efficiency of these modes is how much time is wasted on the long FatSat pulses. When we acquire 4 slices per FatSat, only 39% of the acquisition time is spent on the FatSat module, for 7 slices per FatSat, only 27%.

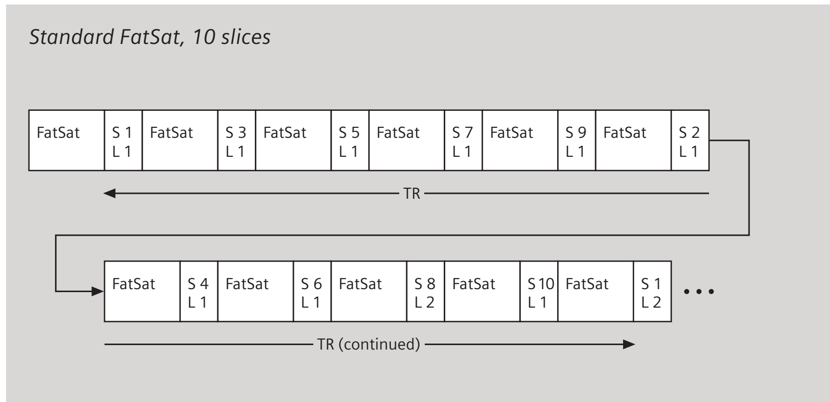

Figure 3 *TR is the duration of ten FatSat pulses and ten imaging modules. As in Figure 1, the FatSat module takes up 72% of the overall imaging time.*

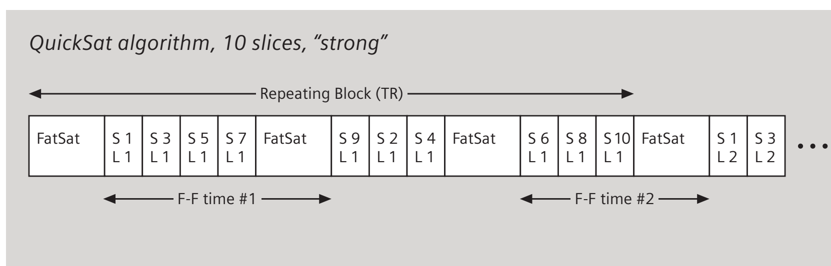

Figure 4 *TR is the duration of three FatSat pulses and ten imaging modules. The FatSat module takes up 44% of the overall imaging time.*

Quick Sat – Large number of slices

The pattern of FatSat and imaging modules changes when we request more slices. Figure 3 shows 10 interleaved slices acquired in standard FatSat mode. The slice numbers represent physical positions, and the interleaving is assumed to be odd slices before even (Fig. 3).

Figure 4 shows 10 interleaved slices in "strong" Quick sat mode. For this example, only 4 slices are permitted after each FatSat pulse (Fig. 4).

The maximum time between FatSat pulses is 50.8 ms, just at the limit for the "strong" algorithm. The TR for any one slice is constant (Rule #2), because the slice only appears once in the repeating block. The TR for all of the slices is the same (Rule #3), because the 10-slice block repeats. The time between a FatSat pulse and a particular slice is constant (Rule #4) for the same reason. The time between the first and the second FatSat pulses is longer than between the other FatSat pulses – this does not cause significant artifacts (Rule #5). It is important to note that slices 1, 9, and 6 are acquired directly following a FatSat pulse, and will show maximal fat suppression. Slices 3, 2, and 8 will show somewhat less suppression, and slices 5, 4, and 10 less still.

Figure 4 should make it clear that the sequence in this example is most efficient when the number of requested slices is a multiple of four, but it is not possible to make the 10-slice sequence more efficient by having four imaging modules between every pair of FatSat modules. Figure 5 shows that the pattern does not repeat after 10 slices.

The first TR for slice 1 is the duration of 10 imaging modules and 2 FatSat modules, but the next TR for this slice is 10 imaging modules and 3 FatSat modules. This violates Rule #2, and would lead to unacceptable artifacts. Rule #4 is also violated.

For quick saturation, "weak" mode gains time efficiency at the cost of a few slices with diminished fat suppression. For the example case, seven imaging modules can be

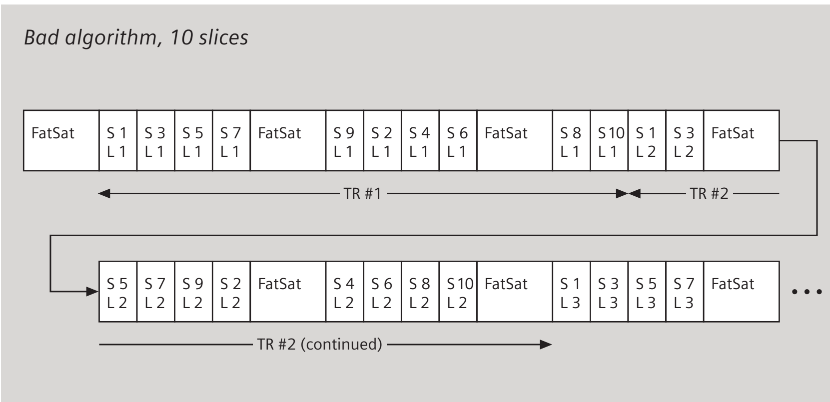

Figure 5 *Four imaging modules are placed between each pair of FatSat pulses. TR #2 continues from the first line to the second.*

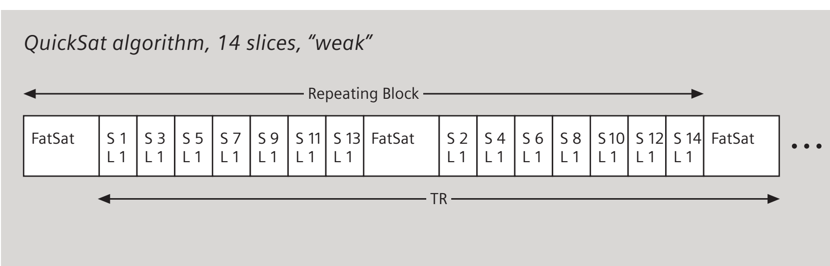

Figure 6 *TR is the duration of two FatSat modules and fourteen imaging modules. Only 27% of the acquisition time is spent for FatSat.*

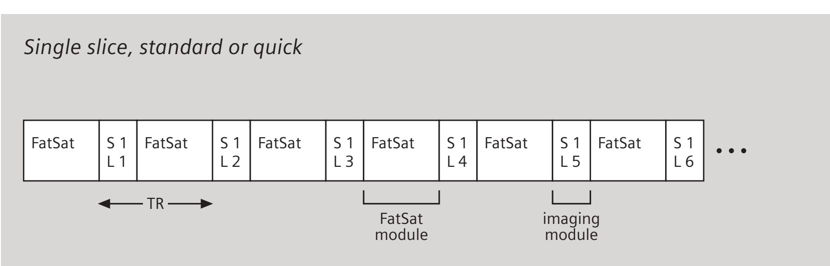

Figure 7 *The only imaging module that could be inserted after slice 1, line 1 would be slice 1, line 2, and this would create Fourier lines with very different TRs (Rule #2), leading to artifacts.*

inserted between the FatSat pulses without exceeding the 75 ms FatSat-to-FatSat limit. Figure 6 shows a 14-slice example.

Note that slices 1 and 2 in the "weak" example of Figure 7 have the same strong fat suppression as slices 1, 9, and 8 in the "strong" example of Figure 4. The only slices in Figure 6 that have weaker saturation than the slices of Figure 4 are slices 9, 11, 13, 10, 12, and 14.

Quick Sat – No "weak" and "strong" for small numbers of slices

The weak and strong modes for quick saturation are only relevant when the number of requested slices is larger than the number that are allowed between FatSat pulses for "strong" mode. For our example, "strong" mode allows as many as four slices between FatSat modules; there is no difference between "weak" and "strong" protocols for 2-, 3-, or 4-slice protocols.

No Quick Sat for single slice

Although permitted by the user interface, there is no Quick sat mode for single-slice protocols. Standard saturation, Quick weak saturation, and Quick strong saturation all follow the pattern of Figure 7.

No Quick Sat for sequential slices

Since sequential slice mode acquires one slice at a time, each slice follows the pattern of Figure 7. Quick saturation is permitted by the user interface (no harm is done), but standard saturation is performed.

Improving slice efficiency for breath-holds

There is a trick that you can use to shorten certain scans by 2-4 seconds.

Quick fat saturation is very useful for time-critical imaging tasks such as breath-hold imaging. To acquire as many slices as possible during the breath-hold, we want to get as many slices between the FatSat pulses as possible. This means using a high receiver bandwidth, the shortest possible TR, and "weak" mode.
For example, using weak mode and a bandwidth of 490 Hz/pixel, it is possible to obtain one Fourier line from 12 slices between the FatSat pulses. With this bandwidth and 114 lines, each additional slice adds 0.5 s to the imaging time, and each FatSat pulse adds 2.16 s. The sequence acquires 12 slices in (12 x 0.5 + 2.16) = 8.16 s, or 1.47 slices per second. The efficiency drops when one more slice (13 total) is requested, because an additional FatSat pulse must be added, and the imaging time is (13 x 0.5 + 2 x 2.16) = 10.82 s, or 1.20 slices per second.

Unfortunately, the maximum number of slices acquired between FatSat pulses varies, depending on how the user types in the number of slices. To obtain the maximum number of slices in the minimum acquisition time for breath-hold applications, use the arrow to increase the number of slices one by one, allowing the system to compute the new TR and acquisition time for each step. You will notice a larger jump in TR and acquisition time when the next FatSat pulse is added. For certain numbers of slices, fewer slices per FatSat will be available when you decrease the number of slices one by one. If you need to decrease the number of slices, reduce the number by at least six slices, reset TR to its minimum value, and begin to increase the number again.

Here are the results for the example above. TR increases by about 4 ms as each slice is added. TR jumps an additional 19 ms as each FatSat pulse is added. The acquisition time is TR times the number of lines. We expect to get 12 slices per FatSat, and we do indeed get 36 slices with three FatSat pulses. However, if we decrease the number of slices to the final value, we can get as few as 9 slices for one FatSat pulse.

Slices	Minimum TR as you increase the no. of slices	Minimum TR as you decrease the no. of slices
1	24	(same) (24)
2	28	(same)
(. . .)		
9	59	(same)
10	63 -------------------------	82
11	68 -------------------------	87
12	91	(same)
(. . .)		
20	126	(same)
21	131	(same)
22	135 ------------------------	154
23	140 ------------------------	159
24	163	(same)
(. . .)		
33	203	(same)
34	207	(same)
35	211 ------------------------	230
36	216 ------------------------	235
37	239	(same)

Quick Sat for 3D MRA Sequences

A different kind of quick saturation is used for some of the 3D angiography sequences in single-slab or sequential slab modes. This allows the acquisition of data for many phase-encoding steps after each FatSat pulse. Because there are fewer 3D (slice) encodings than in-plane (line) encodings, these sequences acquire all of the 3D phase encodings after each FatSat. For a reasonable number of 3D partitions, say 32 or more, it is not possible to maintain good saturation for all of the encodings, so the important central encodings are

acquired first ("centric reordering"). This ensures that large regions of fat are uniformly saturated in all of the reconstructed slices. This is the standard mode of fat saturation for these sequences; the user does not need to select any special "quick" mode.

Quick Sat – Summary

Quick saturation mode is very suitable for breath-hold abdominal examinations, where acquisition speed is much more important than slice-to-slice uniformity of fat suppression.

Conventional FatSat – Strong and weak modes

What are these modes?
For conventional (not Quick) FatSat, "strong" mode gives darker fat than "weak" mode.

Why do we use weak mode ?
Weak FatSat mode prevents the bone marrow from becoming completely black, enabling visualization of marrow lesions. It also keeps the signal from ligaments hypointense. Each slice has essentially the same degree of fat saturation.

With which sequences can we use weak and strong modes ?
"Weak" and "strong" modes are available for RF refocused sequences (SE, TSE, TGSE, and HASTE). Only standard saturation mode is permitted for these sequences; there is no "quick" option. In "strong" mode, an optimized FatSat flip angle is used to ensure the smallest signal from fat. This angle varies with TR and the number of slices. In "weak" mode, a fixed flip angle of 90° is used. Imaging time is the same for both modes.

Standard saturation mode is available for the gradient echo sequences, but only with a fixed FatSat flip angle – there is no "strong" or "weak" option.

Spin Echo "weak" and "strong" versus Gradient Echo "weak" and "strong"

For RF-refocused (SE, TSE, TGSE, HASTE) sequences, "weak" and "strong" adjust the fat brightness of all of the slices together by changing the FatSat pulse tip angle. The strong mode optimizes the tip angle for the number of slices and TR. The weak mode uses a fixed tip angle – the low end of the range of strong values. Except for shim problems, all of the slices for one measurement should have the same fat brightness. Some physicians want very dark bone marrow, and use "strong" mode. Others feel that marrow lesions are more easily seen if the marrow is gray, and use the "weak" mode.

The words "weak" and "strong" have a completely different meaning for the Quick sat mode of the GRE sequence. When many slices are acquired, one group of slices will have good saturation, another group will show less saturation, the next group even less saturation, and so on. In "strong" mode, the slice group showing the least fat suppression will still have relatively good suppression. "Weak" mode allows faster acquisitions, but the slice group showing the least fat suppression will have only adequate suppression. These modes allow the user some choice over this tradeoff. Both "weak" and "strong" modes will give some slices with good saturation, but we cannot use Quick fat sat for consistent control of bone marrow brightness.

MRI Procedures and Transdermal Medication Patches

Frank G. Shellock, Ph.D.

Adjunct Clinical Professor of Radiology and Medicine, University of Southern California and Institute for Magnetic Resonance Safety, Education, and Research
www.MRIsafety.com
www.IMRSER.org

The use of transdermal patches to deliver medications is increasing. A transdermal patch allows continuous and prolonged delivery of a drug that may be more effective and easier than oral medication. In addition, patches offer the potential to deliver medications that would otherwise require injections. Future advances in technology will expand the utilization of drug patches. In fact, researchers are currently working on various technologies, including ultrasound and electrical charges, to force larger molecules through the skin. These so-called "active patches" may permit the delivery of insulin to diabetics, as well as the administration of red-cell stimulating erythropoietin for treatment of anemia patients without injections.

Since 1995, several anecdotal reports have indicated that transdermal patches containing aluminum foil or other similar metallic components may cause excessive heating or a burn in a patient undergoing an MRI procedure. In one incident, a Deponit (nitroglycerin transdermal delivery system) patch, which contains an aluminum foil component, was worn by a patient during MR imaging. The patient received a second-degree burn during an MRI examination performed using conventional pulse sequences and standard imaging procedures (Personal communication, Robert E. Mucha, Schwarz Pharma, Milwaukee, WI; 1995). This injury was likely due to MRI-related heating of the metallic foil associated with this transdermal patch.

The Food and Drug Administration is aware of at least two other adverse occurrences in which patients wearing nicotine transdermal patches during MRI examinations experienced burns. In one case, the patient entered the MR system wearing a Habitrol transdermal patch. When the patient was removed from the scanner after the MRI procedure, he stated that his arm was "burning". Upon examination, his upper left arm appeared to be mildly erythematous and there was a small blister where the patch was located. In another case, a patient underwent a short (less than 40 seconds) MRI examination of the lumbar spine while wearing a nicotine transdermal patch. Later, the patient complained of burn lines on his upper arms associated with the patch.

In view of the above, it is highly recommended that any patient wearing a transdermal patch with a metallic component be identified prior to undergoing MRI. The patient's physician should be contacted to determine if it is possible to temporarily remove the medication patch in order to prevent excessive heating. After the MRI procedure, a new patch should be applied following the directions of the prescribing physician (Personal communication, Robert E. Mucha, Schwarz Pharma, Milwaukee, WI; 1995). Importantly, this procedure should be conducted in consultation with the physician responsible for prescribing the transdermal patch or otherwise responsible for the management of the patient.

The Institute for Safe Medical Practices recently stated that medication patches such as ANDRODERM, TRANSDERM-NITRO, DEPONIT, NICODERM, NICOTROL, CATAPRES-TTS, and possibly others should be removed prior to an MRI examination. In addition, other patches to be aware of include the nicotine patch marketed as Habitrol and its "private label" equivalents and Scopolamine\ Hyoscine HydroBromide, marketed as TransDerm Scop (Personal Communication, 5/19/04, Crispin C. Fernandez, M.D. Medical Affairs, Novartis Consumer Health, Inc. Parsippany, NJ). However, not all medication patches contain a metallic component. Accordingly, these patches do not need to be removed for the MRI examination.

References

http://www.mrisafety.com/
http://www.fda.gov

Institute for Safe Medical Practices, Medication Safety Alert!, Burns in MRI patients wearing transdermal patches. Vol. 9, Issue 7, April 8, 2004. http://www.ismp.org/msaarticles/burnsprint.htm

Shellock FG, Kanal E. Magnetic Resonance: Bioeffects, Safety, and Patient Management. Second Edition, Lippincott-Raven Press, New York, 1996.

Shellock FG. Reference Manual for Magnetic Resonance Safety, Implants, and Devices: Update 2004. Biomedical Research Publishing Group, Los Angeles, CA, 2004.


We see a way to seamlessly image up to 100 cm FoV within a single exam
SIEMENS
MAGNETOM C!
We see a way to position up to 4 coils simultaneously for true multichannel imaging
Small footprint
giant steps
Results may vary. Data on file.
www.siemens.com/medical

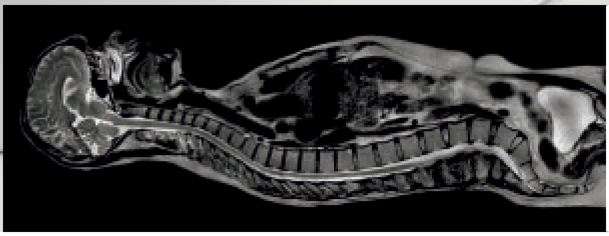

Fast and Ultrafast MR-Sialography

J. Graessner[1], C. R. Habermann[2], M. C. Cramer[2], J. Ussmueller[2], U. Koch[2], G. Adam[2]

[1] Siemens AG Medical Solutions, Hamburg, Germany
[2] University Hospital of Hamburg, Germany

Synopsis

Fast clinical protocols are the backbone of today's clinical routine. We have therefore developed a program of 3 fast and ultra fast 3D TrueFISP and single-shot TSE sequences for the visualization of the regular ductal system of the salivary glands. The resulting image quality of the regular ductal system was so convincing, that pathologic changes should be easily detectable.

Methods

We tried to combine the benefit of a local double-sided surface coil with fast scan times and optimized contrast.

For the ss-TSE sequence we switched to fat suppression via inversion recovery preparation to make the technique more robust against dental implants. Furthermore a reduction in TE time compared to the classical ss-TSE techniques for cholangiography gave more contrast-to-noise.

3 volunteers were examined by using 3D Turbo-Spin-Echo (TSE) with fat saturation (FS) and 2D ss-TSE with inversion recovery (IR) preparation with and without iPAT (integrated parallel acquisition technique; self calibrating GRAPPA (2)). Additionally, we compared the GRAPPA and Sense technique.

For the depiction of the surrounding anatomy we used a segmented 3D TrueFISP with spectral fat saturation. This technique is normally used in cardiac coronary imaging.

All examinations were performed on a MAGNETOM Symphony (Siemens AG, Erlangen, Germany) with 30 mT/m Quantum Gradients and SW version 2002B.

We used the standard CP neck array coil; only the CP element N1 was selected, except for the iPAT ss-TSE measurement, where the lower element of the head coil was selected, to form an iPAT array. The flexible part of the coil was positioned around the mandible with the patient's head in the lower part of the head coil.

The determination of the optimal TI time for fat saturation was done by scanning a set of different TI times from 150 to 400 ms.

A TI time of 280 ms showed best fat suppression (Fig. 5).

The shift of the optimum TI for fat suppression in this setup to 280 ms will be investigated in the future.

Results

Our developed standard protocol included a multiplanar localizer followed by a para-sagittal ss-TSE scan (Fig. 1). The next scan was a 50 mm transverse ss-TSE measurement displaying all four major salivary ducts (Fig. 2). Finally, a transverse 3D TrueFISP (Fig. 3) was performed to detect anatomical changes and pathological masses. An examination time of 5 minutes provides a very comfortable procedure for patients.

The fat saturation with inversion recovery preparation was beneficial compared to the spectral fat saturation due to almost no artifacts from dental implants in the ss-TSE images. iPAT factor = 2 added sharpness to the ss-TSE images by reducing the effective echo-spacing. The GRAPPA technique was much less sensitive to reconstruction-artifacts than the SENSE technique.

TrueFISP was generally less sensitive to metallic implants and insufficient fat saturation because a centrically reordered data-acquisition scheme was used after the fat sat pulse.

The 3D TSE sequence with iPAT and no partial fourier had much better image quality combined with 1.5 mm slice-thickness than the conventional 3D TSE with partial fourier and same scan time. This protocol delivered the thinnest slices, but had the longest scan time without giving further information (Fig. 4).

The 3D TrueFISP protocol also allows slice-thickness far below 2 mm in a reasonable time by decreasing TR and/or increasing the segmentation factor. Interpolation to 512 Matrix enhances the in plane-resolution. A sagittal 3D TrueFISP protocol (Fig. 11) is helpful for anatomical reference.

Conclusions

Showing the ductal system even in healthy volunteers, this protocol is more than sufficient for detection of pathologic changes in patients as proven by the first clinical results (Fig. 6-10).

References

[1] *Becker M, et al. Radiology 2000; 217:347-358.*

[2] *Griswold MA, et al. Proc. of ISMRM/ESMRMB p. 8 (2001).*

[3] *Sakamoto M., et al. Dentomaxillofacial Radiology 2001 30 p.276-284.*

[4] *Jäger L., et al. Radiology 2000; 216:665-671.*

Images of volunteer study (1-4, 11) and of patients (6-10)

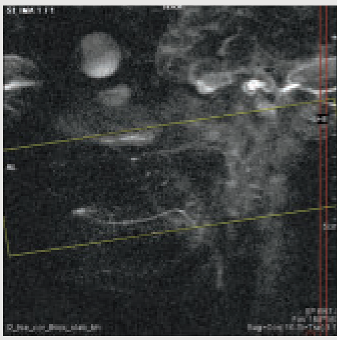

Figure 1 *ss-TSE sagittal localizer.*

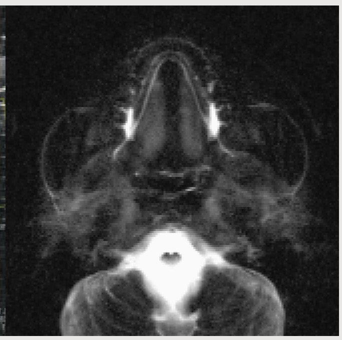

Figure 2 *ss-TSE tra. with iPAT.*

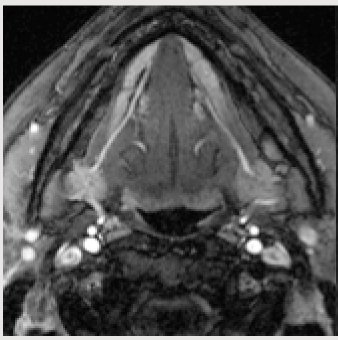

Figure 3 *Segmented 3D TrueFISP.*

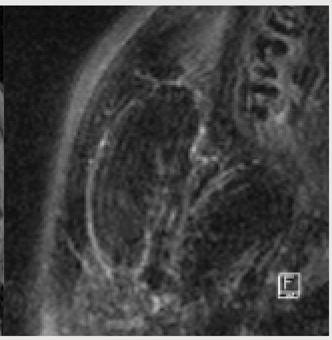

Figure 4 *3D TSE thin MIP.*

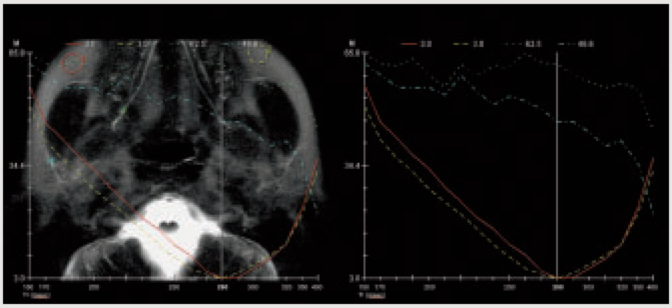

Figure 5 *3D TSE thin MIP.*

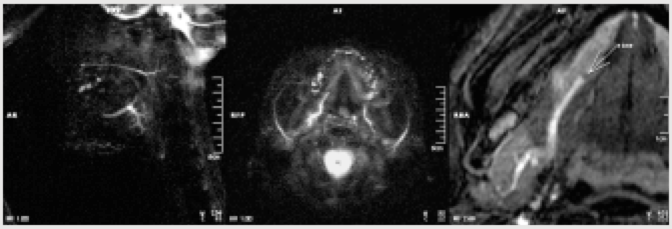

Figure 6,7,8 *Stone in the right main duct; sag-tra ss-TSE, tra 3D TrueFISP.*

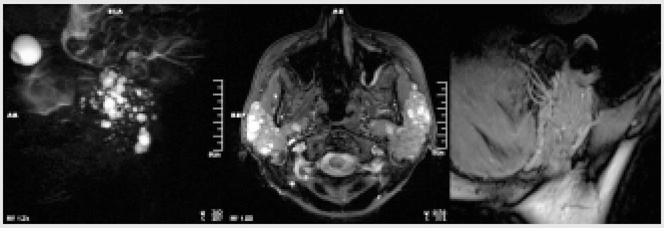

Figure 9,10,11 *Sjögren Syndrome; sag ss-TSE, tra TrueFISP, Normal Parotid.*

Parameters used

Sequence	TR [ms]	TE [ms]	TA [min]	TI/FS [ms]	#SL x Thick	FoV [mm]	Matrix [mm²]	Acq	Turbo Factor/ Segments	Bandwidth [Hz/pixel]
3D TSE	3000	224	3:41	FS	32 x 1.5	160 x 160	251 x 256*	1	65	241
3D TSE iPAT	3000	224	3:41	FS	32 x 1.5	160 x 160	251 x 256	1	65	241
ss-TSE	2800	456	0:03	280	1 x 50	160 x 160	256 x 256	1	256	130
ss-TSE iPAT	2800	456	0:03	280	1 x 50	160 x 160	256 x 256	1	256	130
Seg-3D-TFI	700	2, 29	1:41	FS	24 x 2.5	160 x 160	256 x 256	1	31	570

*using partial fourier in slice and phase encoding direction

Clinical Results with T2_tse_rst_3d_pace_ipat Pulse Sequence

Roger J. Demeure, Ph.D.
Siemens Medical Solutions, Belgium

Nicole Nicaise, M.D.
Centre Hospitalier Universitaire de Charleroi, Belgium

Introduction

With the arrival of

1. the turbo spin echo (tse) with the restore (rst) mode
2. the PACE tool and more recently of
3. the iPAT option, a 3D high resolution free breathing pulse sequence, "tse_rst_3d_ipat", will very soon be available for the routine examinations of millimetric size ducts that lead slow velocity fluids like Wirsung, biliary or salivary ducts.

MR CholangioPancreatography (MRCP)

Techniques: Today, Magnetic Resonance (MR) imaging is the unique modality allowing non-invasive evaluation of the pancreatic ducts, pancreatic parenchyma, adjacent tissues, and vascular network in a single section. In this way, MR CholangioPancreatography (MRCP) is useful for planning surgery or therapic endoscopy and follow-up studies after therapy.

Up to now, MRCP examinations are realized using strongly T2-weighted RARE and HASTE pulse sequences. Both sequences demonstrate the advantages of being very fast and very sensitive to fluids. The RARE pulse sequence allows the acquisition of a single thick section (20-50 mm) in any plane with a single short breath hold (< 3s). Consequently, these pulse sequences are very suitable for investigating the Wirsung and the biliary ducts. Unfortunately, the RARE pulse sequence suffers from some drawbacks. They are 2D pulse sequences requiring slice thickness larger than 20 mm (centrimetric range) which might miss the visualization of small intraductal stones due to the superposition effect. As working under apnea, they require good patient cooperation and strongly depend on the reproducibility of the patient breath holding. Ductal visibility may be degraded by possible overlap with other fluid-containing organs (i.e. stomach and duodenum) and the presence of ascitis or peripancreatic exudates in the field-of-view.

With the arrival soon of the "tse_rst_3d_ipat" all these limitations of the classically used pulse sequences are circumvented for MRCP examinations. This pulse sequence has all the advantages of a regular 3D pulse sequence. Firstly, the improvement in the signal-to-noise ratio leads to a hugely superior in-plane resolution and to a slice thickness (millimetric range) better tuned to the anatomical requirements of the organ under investigation.

Secondly, compared to the regular 2D image acquisition, the richness of the 3D data set provided by "tse_rst_3d_ipat" pulse sequence offers different procedures for reviewing the examination of the biliary and pancreatic system. Indeed, the source images, the "MultiPlanar Reconstruction" (MPR) and the "Maximum Intensity Projection" (MIP) reconstructions are both very helpful because they provide complementary morphologic information. They are better at depicting small or complex anomalities of ducts, i.e. intrahepatic bile ducts stenosis in, for example, "Sclerosing Cholangitis", small intraductal stones, rupture of the Wirsung and post-surgical bile leakage/stenosis.

Furthermore, in the patients with ascitis, the MIP post processing also enables one to get rid of the intraperitoneal liquid which is often more difficult when using the classical RARE pulse sequence. For acquisition time reduction and signal-to-noise optimization, it takes benefit of multi-channel functionality of our system in combination with iPAT. Finally, the last but not the least, this pulse sequence allows to work in free breathing thanks to the PACE (echo navigator) data acquisition synchronization. As already well known, this tool allows the acquisition of images free of motion artifacts in the abdomen without the need of apnea, which is very useful in uncooperative patients.

Results

Acquisition Parameters: the main typical acquisition parameters for the "t2_tse_rst_3d_pace" pulse sequence are : TR/TE_{eff} = 1630 ms/705 ms, Echo Train Length (ETL) = 121, Number of Averages (NA = 1),
Slice Thickness = 1.2 mm, number of slices in the 3D slab = 60, Fat Sat, Band Width = 255 Hz/pxl.

Case 1 (Fig. 1):
This 80 year old non-cooperative woman suffers from pancreatic cancer. The 3D respiratory triggered MRCP nicely emphasizes severe distal stenosis with huge dilation of both biliary and pancreatic ducts. The source images that have a thickness of 1.5 mm allow the exclusion of a microlithiasis.

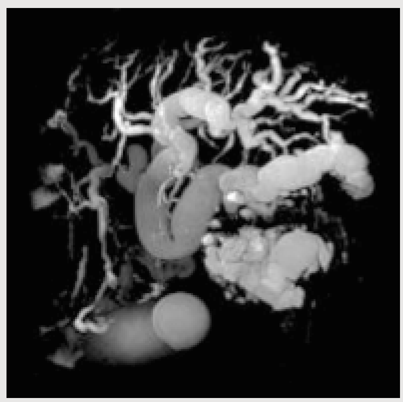
Figure 1.1

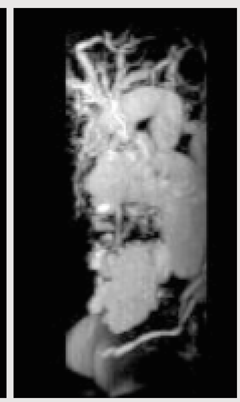
Figure 1.2

Case 2 (Fig. 2):
This 42 year old non-cooperative patient presents with an alcoholic type 4 chronic (induced) pancreatitis. The 3D MRCP nicely depicts the distal stenosis with upstream dilation of both biliary and pancreatic ducts. In addition, a small lithiasis is visible in the t2_tse_rst_3d_pace source images (Fig. 2.3: arrow).

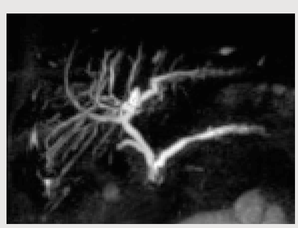
Figure 2.1

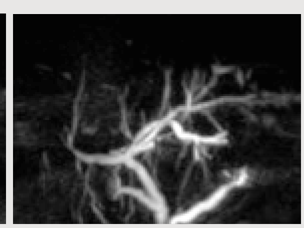
Figure 2.2

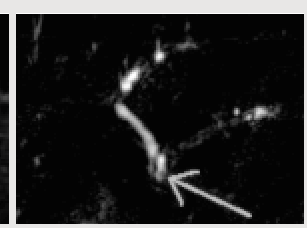
Figure 2.3

Case 3 (Fig. 3):
In this 52 year old patient, the MIP reconstructions nicely depict a distal stenosis of the right intrahepatic biliary duct as well as a post cholecystectomy bile leakage (Fig. 3.3: arrow).


Figure 3.1


Figure 3.2

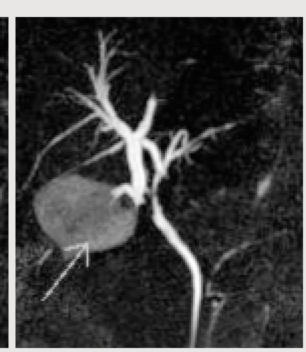
Figure 3.3

Case 4 (Fig. 4):
These MIP reconstructed images were acquired in a 58 year old patient with intraducal papillary mucinous tumor (Fig. 4.2: arrow). The communication between the cystic tumor and the main pancreatic duct is well visualized.


Figure 4.1

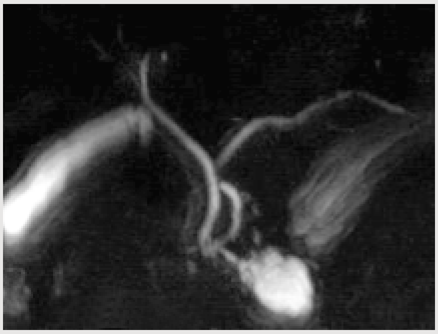
Figure 4.2

Case 5 (Fig. 5):
The examination was done in this non-cooperative 80 year old patient referred for pre-cholecystectomy statement. The MIP reconstructed images depict a low insertion of the cystic duct (Fig. 5).

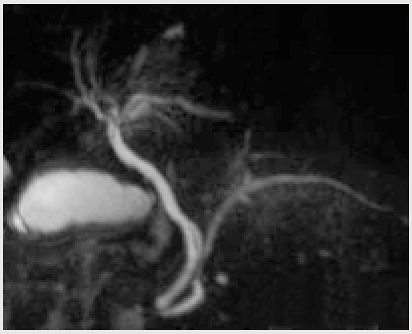
Figure 5

Case 6 (Fig. 6):
This 40 year old patient was referred for pre-cholecystectomy statement. MPR images (1.5 mm thickness) show a gallbladder filled with multiple stones (Fig. 6.1 and Fig. 6.2). Into the thick slice (projections) acquired with the RARE pulse sequence (Fig. 6.2), we suspected stones in the common bile duct. That was excluded thanks to both source and MIP reconstructions.


Figure 6.1


Figure 6.2


Figure 6.3

Urography

Cholangiography is not the only possible application of the "t2_tse_rst_3d_pace" pulse sequence. It could also be very useful for examinations of the urinary system, especially in very young children who are uncooperative and in which the RARE technique is of bad quality. As well known, the poor signal-to-noise ratio produced by the RARE pulse sequence has a direct effect on the minimum possible slice thickness and consequently "t2_tse_rst_3d_pace" could greatly improve the image quality for urography.

In addition, as for MRCP, the analysis of both source images and the MIP/MPR reconstruction increases the diagnostic accuracy of congenital abnormalities, i.e. ectopic ureteral insertion.

Acquisition Parameters: The main typical MR parameters utilized for this kind of examination are:
TR/TE_{eff} = 1910 ms/832 ms,
Echo Train Length (ETL) = 145,
Number of Averages (NA) = 1,
Slice Thickness = 1.5 mm,
Band Width = 260 Hz/pxl.

Results (Fig. 7) :
The MIP images reconstructed from the "t2_3d_tse_rst_pace" data set acquired in this non cooperative 5 year old child provide images of good quality. The multiplanar reconstructions allow to diagnose the correct ureteral insertion.

Other Potential Applications

The current MR data acquisition technique could probably also be used to realize any kind of examination where low velocity fluids are present, like salivary gland channels (sialography).

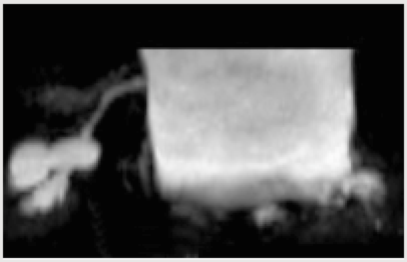

Figure 7.1

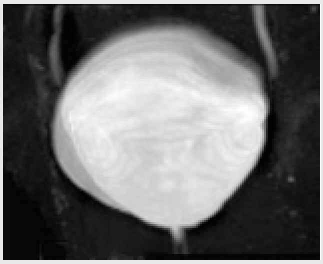

Figure 7.2

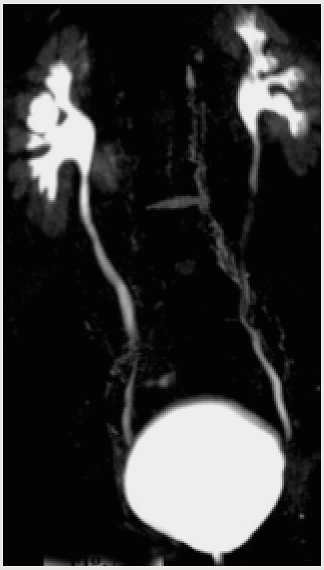

Figure 7.3

Figure 7.4

References

[1] *Atlas of Cross-Sectional and Projective MR Cholangio-pancreatography. L. Van Hoe, D. Vanbeckevoort, W. Van Steenbergen. ISBN 3-540-68831-8, Springer-Verlag (1999).*

[2] *Abdominal and Pelvic MRI. A.L.Baert, K.Sartor, J.E.Youker. ISBN 3-540-67216-8, Springer-Verlag (2000).*

[3] *MR Imaging of the Pancreas : A Pictoral Tour. C.Matos, O.Cappeliez, C.Winant, E.Coppens, J.Devière, T.Metens. 22:2 (2002).*

Upgrade MAGNETOM Vision to MAGNETOM Symphony

Wyncent Wong
MR Applications Specialist
MSc, BAppSc, DCR (R), Dip

Siemens Medical Solutions,
Singapore

Figure 1 *Changi General Hospital.*

Changi General Hospital was officially opened on 28 March 1998 as an amalgamation of Toa Payoh Hospital and Changi Hospital. It is a 800 bed hospital catering specifically for the community in eastern Singapore with an approximate population of 750.000 and offers a comprehensive range of medical and paramedical services. Since the installation of the MAGNETOM Vision in August 1997, the system has scanned an estimated of 15.500 patients before being upgraded to MAGNETOM Symphony Maestro Class on March 2004, making it the first of such upgrades in the region.

With the managed upgrade to MAGNETOM Symphony, all but the magnet was replaced. The gradient strength was increased to 30 mT/m with the true slew rate of 125 T/m/s. Speed is especially significant since the system provides services such as cardiac and abdominal MR in addition to the routine neuro and musculoskeletal MR. Free breathing examinations become a clinical reality with PACE (**P**rospective **A**cquisition **C**or**r****E**ction). PACE is part of Inline Technology, a MAGNETOM Family feature that stands for processing instead of post-processing. Inline Technology processes and reconstructs image data on-the-fly such as motion correction. With the Maestro User Interface performing cardiac MR has never been easier.

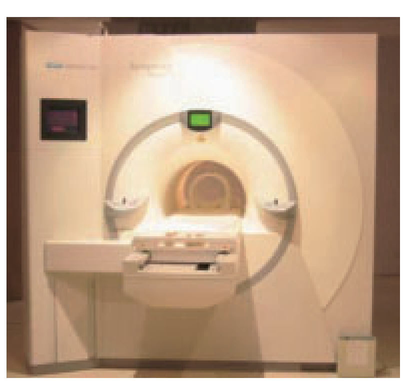

Figure 3 *Whole spine sagittal T1 with Integrated Panoramic Array.*

Figure 2 *MAGNETOM Symphony Maestro Class, a MAGNETOM Vision upgrade.*

Figure 4 *Consultant Radiologist, Dr. Andrew Tan.*

With Maestro Class, iPAT, the **i**ntegrated **P**arallel **A**cquisition **T**echnique is standard and there is no need to purchase additional coils since most of the standard coils are already iPAT compatible.

Dr. Tan, who has a keen interest in body MR, was particularly impressed with the speed of the new system. "With the panoramic table option, performing contrast enhanced MRA of the peripheral vessels has been so much easier. With inline subtraction, it really saves us so much time. I am also very impressed with the restore pulse sequence which was previously not available on the MAGNETOM Vision. It produces very nice T2-weighted spine images with much fewer artifacts." Senior Radiographer in charge – Mr. Salem Koh – agreed that it was definitely the right decision to upgrade the system and that he would strongly recommend such an upgrade. With the MAGNETOM Symphony system, he noticed an increase of 20% in the daily patient throughput.*

But even without a major system upgrade to a new product generation, the Siemens' customer care program – Life – guarantees that the investment in a MAGNETOM system will never become obsolete. The trial programs for coils and application packages, the ongoing training opportunities, and the *syngo* Evolve program™, are all building blocks of Life to help your system match up to the latest standards and enable you to keep up-to-date with the all the applications for the latest techniques in MR.

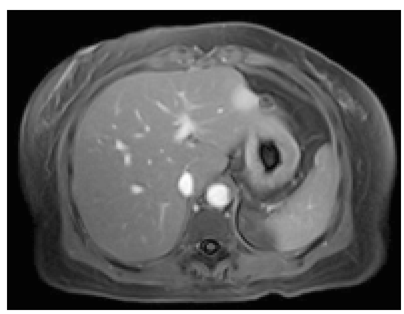

Figure 5 *Turboflash T1 with water excitation and PACE free breathing.*

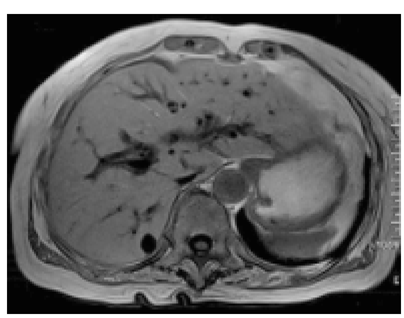

Figure 6 *Flash T1 out of phase*

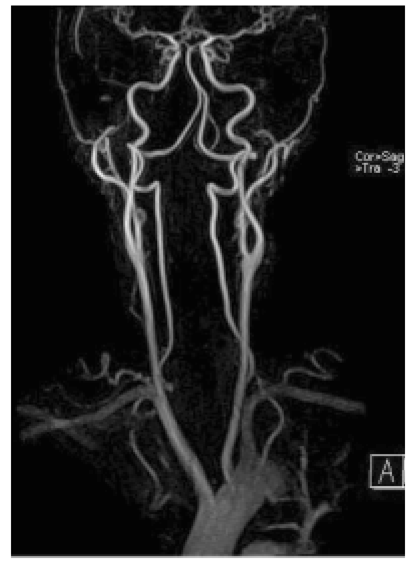

Figure 7 *CE-MRA Carotids.*

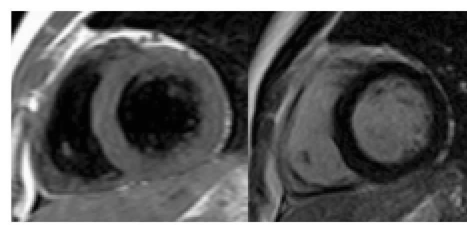

Figure 8 *TSE T2 breath hold and TrueFISP Cine Retrogated.*

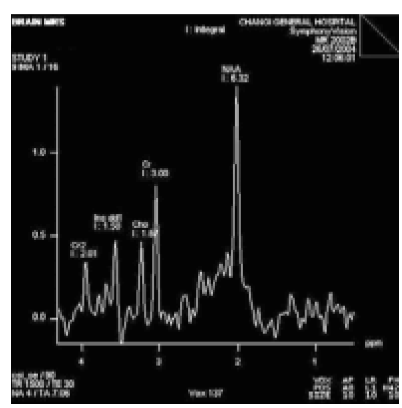

Figure 9 *CSI SE TE 30.*

* *Results may vary. Data on file.*

4^{th} MAGNETOM World Summit September 2005, Singapore

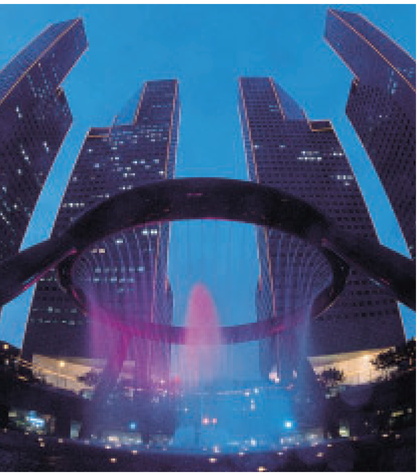

Fountain of Wealth – The largest fountain in the world.

Dear MAGNETOM User,

Welcome to Singapore!

The MAGNETOM World community user meetings provide an excellent opportunity for you to establish personal contacts and exchange valuable information with other users from all over the world. Such a platform will undoubtedly help lay a path for trend-setting developments in MR.

Following our successful meetings in Nice, Miami and our traditional Bavarian event in Rottach-Egern this year, the next MAGNETOM World Summit will take place in Singapore.

For the first time, our Singapore World Summit will integrate the Cardiac MR Ambassador Meeting, the Ultra High-field Meeting and the Low field Meeting. Such a comprehensive agenda and the variety of customers from different backgrounds will make your participation even more worthwhile.

Singapore is truly unique: a dynamic city rich in contrast and color, and a bridge for centuries, it continues to embrace tradition and modernity. We will ensure that our MAGNETOM World members experience another unforgettable event full of stimulation and relaxation in equal measure.

For further information, please contact your Sales Representative or watch out for upcoming news on our MAGNETOM World website at www.siemens.com/magnetom-world.

Best regards,

MAGNETOM World Summit Team

Skyline of Singapore's Central Business District.

Merlion – Half lion, half fish is a national icon.

Vanda Miss Joaquim – Singapore's national flower.

Images courtesy of the Singapore Tourism Board and The Fullerton Singapore.

The information in this document contains general descriptions of the technical options available, which do not always have to be present in individual cases.

The required features should therefore be specified in each individual case at the time of closing the contract.

Siemens reserves the right to modify the design and specifications contained herein without prior notice. Please contact your local Siemens sales representative for the most current information.

Original images always lose a certain amount of detail when reproduced.

This brochure refers to both standard and optional features. Availability and packaging of options varies by country and is subject to change without notice. Some of the features described are not available for commercial distribution in the US.

Siemens AG
Wittelsbacherplatz 2
D-80333 Muenchen
Germany

Headquarters
Siemens AG, Medical Solutions
Henkestr. 127, D-91052 Erlangen
Germany
Telephone: +49 9131 84-0
www.siemens.com/medical

Contact Addresses

In the USA
Siemens Medical Solutions USA, Inc.
51 Valley Stream Parkway
Malvern, PA 19355
Telephone: +1 888-826-9702
Telephone: +1 610-448-4500
Telefax: +1 610-448-2254

In Japan
Siemens-Asahi
Medical Technologies Ltd.
Takanawa Park Tower 14F
20-14, Higashi-Gotanda 3-chome
Shinagawa-ku
Tokyo 141-8644
Telephone: +81 3 5423 8411

In Asia
Siemens Medical Solutions
Asia Pacific Headquarters
The Siemens Center
60 MacPherson Road
Singapore 348615
Telephone: +65 6490-6000
Telefax: +65 6490-6001

In Germany
Siemens AG, Medical Solutions
Magnetic Resonance
Henkestr. 127, D-91052 Erlangen
Germany
Telephone: +49 9131 84-0

Siemens **Medical Solutions** that help

Order No. A91100-M2220-F691-8-7600
Printed in Germany
GP 00000 WS 120420.